Human herpesvirus 8 molecular mimicry of ephrin ligands facilitates cell entry and triggers EphA2 signaling

Taylor P. Light, Delphine Brun, Pablo Guardado-Calvo, Riccardo Pederzoli, Ahmed Haouz, Frank Neipel, Felix Rey, Kalina Hristova, Marija Backovic

▶ **To cite this version:**

HAL Id: pasteur-03259671
https://pasteur.hal.science/pasteur-03259671

Preprint submitted on 14 Jun 2021

1

2

Human herpesvirus 8 molecular mimicry of ephrin ligands facilitates cell entry and triggers EphA2 signaling

5

6

7

8 Taylor P. Light[1], Delphine Brun[2], Pablo Guardado-Calvo[2], Riccardo Pederzoli[2],

9 Ahmed Haouz[3], Frank Neipel[4], Felix Rey[2], Kalina Hristova[1*], Marija Backovic[2*]

10

11

12

13

14 [1] Department of Materials Science and Engineering and Institute for NanoBioTechnology, John Hopkins

15 University, Baltimore, Maryland, USA

16 [2] Unité de Virologie Structurale, Institut Pasteur, Département de Virologie, 28 rue du Dr Roux, 75015

17 Paris, France; CNRS, UMR3569, Paris, France.

18 [3] Crystallography Platform C2RT, Institut Pasteur, 25 rue du Dr. Roux, Paris 75015, Paris, France; CNRS

19 UMR 3528

20 [4] Virologisches Institut, Universitaetsklinikum Erlangen, Schlossgarten 4, D-91054 Erlangen, Germany.

21

22 *Corresponding authors

ABSTRACT

Human herpesvirus 8 (HHV-8) is an oncogenic virus that enters cells by fusion of the viral and endosomal cellular membranes in a process mediated by viral surface glycoproteins. One of the cellular receptors hijacked by HHV-8 to gain access to cells is the EphA2 tyrosine kinase receptor, and the mechanistic basis of EphA2-mediated viral entry remains unclear. Using X-ray structure analysis, targeted mutagenesis and binding studies, we here show that the HHV-8 envelope glycoprotein complex gH/gL binds with sub-nanomolar affinity to EphA2 via molecular mimicry of the receptor's cellular ligands, ephrins, revealing a pivotal role for the conserved gH residue E52 and the amino-terminal peptide of gL. Using FSI-FRET and cell contraction assays, we further demonstrate that the gH/gL complex also functionally mimics ephrin ligand by inducing EphA2 receptor association via its dimerization interface, thus triggering receptor signaling for cytoskeleton remodeling. These results now provide novel insight into the entry mechanism of HHV-8, opening avenues for the search of therapeutic agents that could interfere with HHV-8 related diseases.

INTRODUCTION

Human herpesvirus 8 (HHV-8), also known as Kaposi's sarcoma-associated virus, is a member of *Rhadinovirus* genus that belongs to the *Gammaherpesvirinae* subfamily of *Herpesviridae* [1]. HHV-8 is an oncogenic virus and etiological agent of Kaposi's sarcoma (KS), malignancy of endothelial cells named after the Hungarian dermatologist who first described the disease in 1872 [2]. Because KS has different clinical manifestations, two main forms are distinguished - the classic KS that is a relatively indolent and rare tumor, appearing as skin lesions mostly in elderly men, and the epidemic or HIV-associated KS, an aggressive form that spreads extensively through skin, lymph nodes, intestines and lungs [3]. The KS affects up to 30% of untreated HIV-positive individuals [4,5], and is nowadays one of the most frequent malignancies in men and children in subequatorial African countries [6].

Behind the ability of HHV-8 to spread to diverse tissues lies its wide tropism demonstrated *in vivo* for epithelial and endothelial cells, fibroblasts, B- and T-lymphocytes, monocytes, macrophages and dendritic cells (reviewed in [7]). As other herpesviruses, HHV-8 attaches to cells via its envelope glycoproteins that engage in numerous low affinity interactions with ubiquitous cellular factors such as heparan sulfate proteoglycans [8]. Following these initial contacts, the viral envelope glycoprotein(s) bind to specific cell receptor(s) in an interaction that provides trigger for membrane fusion. The envelope glycoproteins B (gB) and the non-covalent heterodimer made of glycoproteins H and L (gH/gL) constitute the conserved core fusion machinery of all herpesviruses, whose function is to induce merger of the viral and cellular membranes. The release of herpesvirus capsids occurs at the level of plasma membrane or as in the case of HHV-8, after endocytosis, by fusion of the viral and endosomal membranes [9]. In all herpesviruses gB is the fusogen protein, while gH/gL plays a role in regulation of gB activity [10]. What is particular to HHV-8 is the simultaneous employment of several viral glycoproteins - HHV-8-specific K8.1A glycoprotein, as well as the core fusion machinery components – that engage diverse cellular receptors (gB binds to integrins and DC-SIGN, gH/gL to EphA receptors) increasing the HHV-8 target repertoire and providing the virus with a set of tools for well-orchestrated entry (reviewed in [11]).

The X-ray structures of gH/gL from alpha-, beta- and gammaherpesviruses [12-15], revealed a tightly bound protein complex, in which the gH ectodomain, composed of four domains forms a tight complex with gL via its N-terminal, membrane-distal domain. Despite low gH and gL sequence conservation across the herpesvirus family, the structures are remarkably similar, indicating conservation of a function. The current fusion model posits that upon binding of the virus to the cellular receptor (via gH/gL, gB, or a virus-specific glycoprotein), gH/gL in a still unknown way relays the signal and switches gB fusion activity on, setting membrane fusion in motion [16]. As mentioned above, HHV-8 gH/gL also functions as a receptor binding protein that interacts with cellular Eph

71   receptors that belong to a superfamily of transmembrane tyrosine kinases, named Eph for their

72   expression in erythropoietin-producing human hepatocellular carcinoma cell line [17].

73   The physiological ligands of Eph receptors are membrane-tethered proteins called ephrins

74   (acronym for Eph family receptor interacting proteins). Ephrin-A ligands are attached to the membrane

75   by glycosylphosphatidylinositol anchors and bind to Eph receptors classified as type-A Eph receptors,

76   while ephrin-B ligands possess a transmembrane and an intracellular PDZ domain and interact with

77   receptors designated as Eph type-B receptors [18,19]. There are 5 ephrin-A ligands and 9 Eph type-A

78   receptors in humans. HHV-8 binds with the highest affinity to EphA2, and less to the related EphA4

79   and EphA7 receptors [20-22]. In addition, the EphA2 receptor serves as a receptor for two other

80   gammaherpesviruses - human herpesvirus 4 (HHV-4 also known as Epstein-Barr virus (EBV) and rhesus

81   monkey rhadinovirus [23,24]. The interactions are in all cases established via gH/gL. Unrelated pathogens

82   such as Hepatitis C virus, some bacteria and yeast also depend on EphA2 receptor for entry [25-28].

83   Eph receptor-ephrin ligand interactions mediate short-distance cell-cell communications and

84   lead to cytoskeleton rearrangements and rapid changes in cell mobility and / or morphology [29]. Some

85   of the typical outcomes of ephrin-A1 ligand activation of EphA2 receptor are cell retraction [30-33] and

86   endocytosis of receptor-ligand complexes [34]. These processes are especially active and important

87   during development, and in adulthood many of the same circuits get repurposed for functions in bone

88   homeostasis, angiogenesis, synaptic plasticity (reviewed in [29]). Since motility and angiogenesis

89   contribute to tumorigenesis and other pathologies, Eph receptors and ephrin ligands are in the

90   spotlight as targets for therapeutic intervention [35,36].

91   EphA2 was identified as HHV-8 entry receptor by Hahn *et al*. who showed that deletion of the

92   EphA2 gene abolished infection of endothelial cells, and that binding of gH/gL to EphA2 on cells led to

93   increased EphA2 phosphorylation and endocytosis facilitating viral entry. The presence of the

94   intracellular kinase domain was shown to be important for HHV-8 entry in epithelial 293 cells [20]. In

95   this respect, HHV-8 gH/gL does not play the role of a classical herpesvirus receptor binding protein,

96   directly activating gB upon binding to a cellular receptor to induce fusion of the viral and plasma

97   membranes, such as gD in alphaherpesviruses. The merger of the HHV-8 and cellular membranes

98   occurs at low pH within an endosome, and is spatially and temporally separated from the gH/gL

99   interactions with EphA2 that occur at the cell surface. HHV-8 gH/gL instead activates EphA2 receptors

100 that initiate signaling pathways leading to rapid internalization of the virus and cytoskeletal

101 rearrangements that create a cellular environment conducive for the virus and capsid intracellular

102 transport [37].

103   All Eph receptors contain an elongated ectodomain made of – as beads on a string - a ligand-

104 binding domain (LBD), a cysteine-rich domain (CRD) and two fibronectin (FN) domains, followed by a

105 transmembrane anchor, a short juxtamembrane region containing several conserved tyrosine

106 residues, an intracellular Tyr kinase domain, a sterile alpha motif (SAM) that has a propensity to

107   oligomerize, and a PDZ domain involved in protein-protein interactions [38]. The LBD consists of a rigid,

108   conserved β-sandwich, decorated with variable loops that dictate ligand specificity [39,40]. In a similar

109   fashion, the protruding flexible loops of ephrin ligands are arranged around a compact, eight-stranded

110   central β-barrel [41]. We employ the accepted nomenclature for the secondary structure elements for

111   Eph receptors [42] and ephrin ligands throughout the text [41]. In both cases single letters designate β-

112   strands and helices, and double letters are used to label loops that connect the secondary structure

113   elements (Fig. S1). The ephrin ligand interactions with the Eph receptors are driven by an 18-residue

114   long and mostly hydrophobic loop that connects strands G and H – the GH loop – of the ligand, which

115   inserts into a complementary hydrophobic cavity presented at the surface of the receptor LBD [42]. The

116   ephrin ligand GH loop carries a conserved E119 that establishes polar interactions, critical for high

117   affinity binding, with a strictly conserved R103 on the loop of the Eph type-A receptors. This R103

118   happens to be in the loop connecting strands G and H in EphA receptors and is also designated as GH

119   loop [43]. To avoid confusion, we use superscripts to indicate the molecule of the residue or feature

120   described (R103^{EphA2}, E119^{ephrin}, GH^{EphA2}, GH^{ephrin} etc).

121   At the molecular level, as in the case of other receptor tyrosine kinases, ephrin ligand binding

122   induces oligomerization of Eph receptors, promoting trans-phosphorylation and signal transduction

123   into the cell [19]. Structural and functional studies revealed that ephrin ligand binding to Eph receptors

124   results first in formation of so-called tetramers made of two 'Eph-ephrin' complexes in which each Eph

125   receptor interacts with 2 ephrin molecules – its cognate ligand with high affinity, and via low affinity

126   interactions with ephrin from the other complex [18] (Fig. S2). In such tetrameric arrangement that is

127   brought about by ligands, two Eph receptors are arranged into a dimer (also known as homodimer),

128   stabilized by contacts at the EphA2 LBD dimerization interface (DIN). Eph-ephrin tetramers can

129   polymerize into clusters via the interface in the downstream CRD referred to as the clustering interface

130   (CIN) [44-46]. Since the clustering involves an EphA2 region outside of the LBD, this interface is known as

131   ligand independent. Indeed EphA2 receptor was shown to exist on cells in the absence of ligand in a

132   monomer-dimer equilibrium [47], with the unliganded dimers stabilized via the CIN (Fig. S2).

133   The cellular response to EphA2 receptor activation is ligand- and cell-type dependent and

134   modulated by factors such as the spatial distribution of the receptor in the membrane [48], residues in

135   the intracellular domain that are phosphorylated, size and type of the EphA2 receptor oligomers, to

136   just name some [29]. EphA2 receptor dimers were shown to be already active [49], and there is evidence

137   that oligomers made of 6-8 EphA2 receptor molecules activate, while larger aggregates may dampen

138   the signaling in some cell types [50]. Different ligands (monomeric, dimeric ephrin-A1, and agonist or

139   antagonist peptides) were shown to stabilize distinct dimeric or oligomeric EphA2 receptor assemblies

140   (Fig. S2), further indicating that the signaling properties may be defined by the nature of the EphA2

141   dimers and oligomers [47,51].

142   The structures of several Eph receptor – ephrin ligand complexes have been determined

143   [39,40,42,44,45], but how viral antigens such as HHV-8 gH/gL interact with EphA2 was completely unknown

144   until recently. The 3.2Å X-ray structure of a HHV8 gH/gL-EphA2 complex was published while we were

145   preparing this manuscript [52]. Our goal has been to explore the events that emulate the early stages of

146   HHV-8 entry. We south to obtain the structural details on the gH/gL-EphA2 complex, and to determine

147   if and how HHV-8 gH/gL affects assembly of EphA2 receptors in the membranes of living cells, taking

148   advantage of the FSI-FRET system that allows following lateral interactions of membrane proteins *in*

149   *vivo* [53]. We report here a 2.7Å resolution X-ray structure of the HHV-8 gH/gL ectodomain bound to the

150   LBD of EphA2 together with results of structure-guided mutagenesis and cell-based studies that

151   highlight E52^{gH} as a key residue for high-affinity binding to the receptor. Based on our analyses and the

152   similarities we observed between the binding modes of gH/gL and the ephrin ligand to EphA2, we

153   provide evidence that this structural similarity extends into functional mimicry - soluble gH/gL induces

154   cell contraction and stabilizes the same type of EphA2 receptor dimers on cells, as was shown for the

155   ephrin-A1 ligand [47]. This is the first time that a non-ephrin protein in its monomeric form has been

156   shown to activate Eph receptors, underscoring that signaling via EphA2 dimers, and not large

157   oligomers, may be more common than thought. The results presented here now lay a path for further

158   exploration of downstream events and the investigation of whether HHV-8 activation of Eph receptors

159   may play a role beyond ensuring a productive infection, for example contributing to virus

160   oncogenicity/oncogenic transformation of the cell.

RESULTS

Structure determination of the EphA2 LBD - gH/gL tertiary complex

Recombinant HHV-8 gH/gL ectodomains and EphA2 LBD were expressed in insect cells and the proteins were purified as described in detail in Material and Methods (MM). To maximize the tertiary complex (gH/gL-bound to EphA2 LBD) formation, the gH/gL was mixed with an excess of LBD which was then removed by size exclusion chromatography. Multiangle light scattering measurements [54] demonstrated a 1:1:1 tertiary complex stoichiometry for gL/gH bound to EphA2 LBD, as well as to the EphA2 ectodomain (Fig. S3).

The tertiary complex crystallized in an orthorhombic space group (C 2 2 2_1) and the crystals, which contained one molecule per asymmetric unit, diffracted to 2.7Å. The initial phases were calculated by molecular replacement using the EphA2 LBD (PDB: 3HEI) and an HHV-8 gH/gL theoretical model derived from the EBV gH/gL X-ray structure (PDB: 3PHF) using the Phyre2 program for protein modelling and structure prediction [55]. The partial molecular replacement solution was extended by iterative cycles of auto- and manual building as explained in MM. The final map displayed clear electron density for residues 27-200 of EphA2, residues 21-128 for gL, and residues 35-696 gH with the exception of several short regions of poor density that precluded unambiguous placement of the polypeptide chain (Fig. 1A). The N-terminus of gL contained two additional residues (Arg and Ser) carried over from the expression vector. Around 40 gL residues at its C-terminus were not resolved and are likely to be disordered as predicted by IUPred2A server [56,57]. The atomic model was refined to a R_{work}/R_{free} of 0.22/24 (Table S1).

The gH/gL-EphA2 LBD complex structure

The tertiary complex forms an extended structure 15 nm long and around 4.6 nm across its widest part, in the gH region (Fig. 1B). EphA2 LBD adopts a jelly-roll fold as originally described [39] – its N- and C-termini point in the same direction and away from the gH/gL binding site, consistent with the expected location of the remaining EphA2 domains. Two antiparallel 5-stranded β-sheets pack into a compact β-sandwich, with loops of different lengths connecting the strands. The HI[EphA2] loop is well ordered and forms the DIN, while the JK[EphA2] loop, which carries a short J' helix, is not resolved in our tertiary complex structure likely due to its already reported structural plasticity [40] and / or displacement by gL (Fig.1B). Apart from the JK[EphA2] loop, the EphA2 LBD does not change conformation upon binding to gH/gL.

The gH/gL complex has an architecture already described for other herpesvirus orthologs – the γ-herpesvirus EBV gH/gL [15], β-herpesvirus human CMV [13], and α-herpesviruses HSV-2, PrV and VZV [14,58,59].

7

195   The N-terminal domain I (DI) of gH is separated by a linker (hinge) helix from the rest of the ectodomain

196   (domains II, III and the membrane-proximal domain IV) (Fig. 1B). The HHV-8 gH/gL resembles the most

197   its EBV counterpart, consistent with the highest sequence conservation between the two, followed by

198   the β-herpesvirus CMV gH/gL complex and less so the α-herpesvirus complexes (Fig. S4). The rmsd

199   values and Z-scores calculated from the superimposition of individual gH domains and gL are given in

200   Fig. S4 (superimposing the entire gH/gL ectodomains is not informative because of the different

201   orientations of the domains with respect to each other). Clear electron density was observed at 4 N-

202   linked glycosylation sites (N46^{gH}, N267^{gH}, N688^{gH}, and N118^{gL}) allowing placement of 1 or 2 N-

203   acetylglucosamine residues.

204

205   Binding interface between gH/gL and EphA2

206   The EphA2 LBD and gH/gL form an intricate interface structure made of a seven-stranded

207   mixed β-sheet containing strands contributed by all 3 proteins. The N-terminal segment of gH co-folds

208   with gL forming a mixed five-stranded β-sheet composed of two gH and three gL β-strands. The third

209   gL β-strand further engages in contacts with the D β-strand of EphA2 (Fig. 2A).

210   gL binds to the EphA2 LBD via its N-terminal segment (residues 21-30) and residues from its

211   β2 and β3 strands (Fig. 2A) (the full list of contact residues is given in Table S2 and is represented in

212   Fig. S5). The gL N-terminal segment is restrained by C26 and C27 that form disulfide bonds with C74

213   and C54, respectively. Immediately upstream this anchoring point there is an elongated, hydrophobic

214   'tail' (residues 21-25) that inserts into a hydrophobic channel formed by the EphA2 strands D and E

215   and gL strands β2 and β3 (the 'roof'). The buried surface area for the gL residues 19-32 is around 480

216   Å^2. Of the 14 hydrogen bonds formed between gL and EphA2, 7 are contributed by the gL N-terminal

217   segment, 6 by strand β3 and 1 by the C-terminal η4 Asn128.

218   Below the gL 'tail', the single gH residue that makes contacts with EphA2 – E52^{gH} – forms a salt

219   bridge with R103^{EphA2}, clamping the bottom of the tunnel (the 'base'). E52^{gH} is also involved in polar

220   interactions with residues V22^{gL}, H47^{gL} and F48^{gL}, thus being a center point (a hub) interlaying gL and

221   EphA2 (Table S2).

222

223   Biolayer Interferometry (BLI) analyses of EphA2 and gH/gL interactions in solution

224   To investigate the role of the gH/gL and EphA2 residues implicated in the interactions observed

225   in the crystal structure, we tested a series of mutants that were conceived to induce large

226   perturbations into gL and EphA2 by introducing N-glycosylation sites. We resorted to such drastic

227   changes because most EphA2 point mutations already tested in immunoprecipitation assays had only

228   moderate effects on gH/gL binding [60]. The point mutation R103A^{EphA2} has been reported to abolish the

229   binding to gH/gL [52] and served as a positive control. Since E52^{gH} is the only gH residue contacting EphA2,

230   we also introduced point mutations E52A^{gH} and E52R^{gH} to specifically target this site.

231   The variants with the following N-glycosylation sites were generated: N57^{EphA2}, N190^{EphA2},

232   N30^{gL} or N68 ^{gL}, and point mutant variants R103A^{EphA2}, E52A^{gH} bound to gL (E52A^{gH}/ gL) and E52R^{gH}/ gL

233   (Fig. 2B). The recombinant proteins were expressed in mammalian cells. The introduced sites N30^{gL}

234   and N68 ^{gL} were glycosylated as clearly observed by gL shift to a higher molecular weight on SDS-PAGE

235   gels, while the change in the migration was harder to detect for EphA2 ectodomains possibly because

236   its larger size and small difference introduced by an additional glycosylation. The N190^{EphA2} mutation

237   was already reported to perturb the interactions with ephrin ligands [44]. The constructs were

238   engineered so that gL contained a strep tag for complex purification, as before, and gH contained a

239   histidine tag at C-terminus for immobilization onto BLI sensors via the end distal to the EphA2 binding

240   site (Fig. S6). Further details on protein production and BLI parameters are given in MM.

241   We determined the dissociation constant (Kd) <1nM by doing a series of BLI measurements

242   for wild type (WT) gH/gL binding to the EphA2 ectodomain (res. 27 - 534) or its LBD (res. 27-202) (Fig.

243   2C). The low Kd observed for the WT proteins was dominated by a slow k_{off} rate. We obtained a Kd in

244   the subnanomolar range when the measurements were done at pH 5.5 (Fig. S7A), or when the system

245   was inverted i.e. EphA2 LBD or ectodomains were immobilized via a histidine-tag to the sensor, and

246   gH/gL was in solution (Fig. S7B).

247   Each of the 3 mutations introduced in EphA2 significantly reduced the binding as anticipated

248   (Fig. 2D). The Q30N^{gL} mutation in the gL N-terminal segment also diminished binding, consistent with

249   the presence of a carbohydrate at this position blocking the interactions with the strand D^{EphA2} and

250   DE^{EphA2} loop. Introduction of the N-linked carbohydrate at residue N68^{gL} in its β2-β3 turn did not affect

251   binding as expected, because of its location proximal to the binding site but in an exposed loop (Fig.

252   2B). The E52R^{gH}/gL and E52A^{gH}/gL variants resulted in weaker or absence of interactions with EphA2

253   ectodomains, respectively (Fig. 2D). These results demonstrated that the binding interface between

254   EphA2 and gH/gL seen in the crystal is in agreement with the one mapped by measurements in

255   solution.

256

257   The gH/gL molecular mimicry of ephrin-A ligands

258   The EphA2 binding site for ephrin-A1 ligand and gH/gL largely overlap, with the former

259   including a more extensive surface area and a larger number of contacts established by EphA2 β-

260   strands D and E, CD and DE loops, as well as the LM loop (Fig. 3, Fig. S1 and S5). Comparative analyses

261   of the gH/gL-EphA2 and ephrin-A1-EphA2 complexes further demonstrate that the structural elements

262   employed by gH and gL resemble the ephrin-A1 ligand mode of binding to EphA2 receptor. The GH$^{ephrin-}$

263   ^{A1} loop, which is the principal interaction region with the EphA2 receptor, occupies the same space as

264 the gL 'tail', while the salt bridge established between the conserved R103^{EphA2} and E119$^{ephrin-A1}$ is

265 replaced at the same location by a salt bridge between R103^{EphA2} and E52^{gH} (Fig. 3). The conserved

266 E52^{gH} and E119$^{ephrin-A1}$ occupy equivalent position in respect to R103^{EphA2}, but the chain segments

267 carrying the conserved E52^{gH} and E119$^{ephrin-A1}$ run in opposite directions so that the following residues,

268 F53^{gH} and F120$^{ephrin-A1}$, do not superpose. Both F53^{gH} and F120$^{ephrin-A1}$ are engaged in π-π stacking

269 interactions with F108 $^{ephrin-A1}$ and H53^{gL}, respectively; in addition, the F108^{EphA2} establishes π-π

270 interactions with Y21^{gL} or F111$^{ephrin-A1}$, indicating a common mechanism for stabilization of the loop

271 that presents the critically important glutamic acid residue for interactions with EphA2.

272

273 HHV-8 gH/gL induces constitutive EphA2 dimerization on the cell surface

274 Since binding of ephrin ligands to Eph receptors induces formation of higher-order receptor

275 oligomers, we sought to determine if gH/gL alters EphA2 interactions at the cell surface in a similar

276 fashion. The method we applied was developed to probe the stability and association (stoichiometry)

277 of protein complexes in cell membranes, and is referred to as FSI-FRET (Fully Quantified Spectral

278 Imaging (FSI) Förster Resonance Energy Transfer (FRET)) [53]. The measurements are carried out on the

279 membranes of live cells containing the proteins of interest tagged with donor or acceptor fluorescent

280 probes at the intracellular end. The lateral interactions of EphA2 molecules in the absence and

281 presence of various ligands were already investigated using this approach [47].

282 We performed FSI-FRET measurements in HEK293T cells co-transfected with EphA2-

283 mTurquoise (donor probe) and EphA2-eYFP (acceptor probe). Recombinant HHV-8 gH/gL was added

284 at the final concentration of 200 nM, significantly exceeding the apparent subnanomolar Kd value (Fig.

285 2C), thus ensuring that all the EphA2 molecules were occupied by gH/gL. The measured FRET

286 efficiencies (corrected for "proximity FRET" as discussed in MM (equation 1), and the concentration of

287 donor-tagged and acceptor-tagged EphA2 molecules) were used to construct dimerization curves by

288 fitting with a monomer-dimer equilibrium model [53] (the raw FRET data is shown in Fig. S8). Dimer

289 formation is characterized by two parameters: the two-dimensional dissociation constant, $K_{diss,}$ and

290 the structural parameter "Intrinsic FRET", $\tilde{E}$. The K_{diss} is a measure of the dimerization propensity of

291 EphA2 at the plasma membrane. The Intrinsic FRET is the FRET efficiency in an EphA2 dimer with a

292 donor and an acceptor, which depends on the positioning of the fluorescent proteins (attached to the

293 C-terminus of the intracellular domain) of the EphA2 dimer. The Intrinsic FRET is strictly a structural

294 parameter and therefore does not have any implications on the dimerization propensity of the full

295 length EphA2 receptor [64, 65].

296 The dimerization curve calculated from the FRET data for EphA2 WT in the presence of gH/gL

297 is shown in Fig. 4A and is compared to the data for EphA2 WT in the absence of ligand. The best-fit K_{diss}

298 and the best-fit Intrinsic FRET, determined from the FRET data, are presented in Table 1. As previously

299   reported [51], EphA2 WT in the absence of ligand exists in monomer-dimer equilibrium with a K_{diss} is 301

300   ± 67 receptors/μm². We found EphA2 in the presence of gH/gL to be 100% dimeric ("constitutive

301   dimer") over the EphA2 concentration range observed in the experiments, precluding reliable

302   measurement and calculation of the dissociation constant. In control experiments, we added soluble

303   EphA2 LBD and also precomplexed gH/gL with EphA2 LBD (gH/gL-LBD) (Fig. 4B, C). As anticipated,

304   soluble LBD had no effect on EphA2 dimerization and the effect of gH/gL was also abolished when

305   precomplexed with EphA2 LBD, as the dimerization curves and the best-fit K_{diss} value were

306   indistinguishable from those determined in the absence of gH/gL (Table 1).

307   Along with K_{diss}, which measures the strength of the EphA2 association, these experiments give

308   information about conformational changes that affect the relative disposition of the fluorescent

309   proteins attached to the C-termini of EphA2, inside the cell. This information is contained in the

310   structural parameter "Intrinsic FRET". A lower Intrinsic FRET value is observed upon gH/gL binding,

311   reflecting that the distance (d) between the fluorescent proteins is greater when gH/gL is bound to

312   EphA2. Since the fluorescent proteins are attached to the C-termini of EphA2 via flexible linkers, this

313   is a demonstration of a structural change in the EphA2 dimer induced by gH/gL binding, which is

314   transmitted across the membrane to the intracellular domains, involving an apparent increase in the

315   separation between the C-termini of EphA2. This implies that the conformation of the intracellular

316   domains in the EphA2 dimer are altered in response to gH/gL binding. The presence of soluble EphA2

317   LBD and precomplexed gH/gL-LBD had no effect on the Intrinsic FRET values (Table 1).

318   Since FRET has limited utility in discerning the oligomer size, we used Fluorescence Intensity

319   Fluctuation (FIF) to directly assess the oligomer size of EphA2 in the presence of gH/gL. FIF calculates

320   molecular brightness of eYFP-tagged receptors in regions of the cell membrane. The molecular

321   brightness, defined as the ratio of the variance of the fluorescence intensity within a membrane region

322   to the mean fluorescence intensity in this region, is known to scale with the oligomer size [61]. The

323   cumulative (over all measured EphA2 concentrations) distributions of molecular brightness for EphA2

324   and EphA2 with gH/gL obtained from small sections of the plasma membrane in hundreds of cells are

325   compared in Fig. 4D. Consistent with the fact that EphA2 exists in a monomer/dimer equilibrium in the

326   absence of ligand [51], the EphA2 brightness distribution is between the distributions of LAT (Linker for

327   Activation of T-cells, a monomer control) [62] and E-cadherin (a dimer control) [63]. The FIF data for these

328   controls have been published previously [64] and are shown here for comparison (Fig. 4D). We found

329   that gH/gL shifts the maximum of the histogram to higher molecular brightness relative to EphA2

330   (untreated), such that it virtually overlaps with the dimeric E-cadherin distribution. Therefore, the FIF

331   measurements indicate that EphA2 is a constitutive dimer in the presence of gH/gL, consistent with

332   the FRET data. We see no indication for the formation of higher order oligomers, which would have

333   resulted in a brightness distribution shifted to higher values than the ones measured for E-cadherin.

334   Taken together, the FRET and FIF data demonstrate that gH/gL significantly stabilizes EphA2 dimers

335   but does not induce EphA2 oligomerization.

336

337   Residues E52^{gH} and R103^{EphA2} are critical for EphA2 dimerization on cells

338   To test the importance of residue E52^{gH} for binding of gH/gL to EphA2 in native membranes,

339   FSI-FRET experiments were also performed with the E52R^{gH}/gL recombinant protein, which exhibited

340   significantly reduced binding to the soluble EphA2 ectodomains in BLI experiments (Fig. 2D). The

341   dimerization curve for EphA2 WT in the presence of E52R^{gH}/gL is shown in Figure 5A and the fit

342   parameters in Table 1. Constitutive EphA2 receptor dimerization was not observed as we did with

343   gH/gL. Rather, EphA2 interactions were reduced to levels similar to the case of no ligand, indicating

344   that the presence of E52R^{gH}/gL did not result in EphA2 dimer stabilization. This is consistent with the

345   finding that the binding of this E52R^{gH}/gL variant to EphA2 was disrupted, and/or with the idea that

346   bound E52R^{gH}/gL did not enhance dimer stability. However, the measured Intrinsic FRET was slightly

347   increased, as compared to no treatment, suggesting a decrease in the separation between the

348   attached fluorescent proteins, and thus between the C-termini of EphA2. This effect could be due to

349   structural perturbations in the EphA2 dimer in response to possible E52R^{gH}/gL binding at the high

350   E52R^{gH}/gL (200nM) concentrations used, which could have propagated to the intracellular domain of

351   EphA2.

352   In addition, we sought to test the importance of the residue R103^{EphA2} for binding to gH/gL

353   using the FSI-FRET method. The dimerization curve when the cells were transfected with EphA2

354   harboring the R103E mutation in the gH/gL binding site, in the presence of saturating gH/gL

355   concentrations, is shown in Fig. 5B, and the fit parameters are shown in Table 1. The dimerization

356   propensity for R103E^{EphA2} variant in the presence of gH/gL is the same as for EphA2 in the absence of

357   ligand (Table 1), indicating that either gH/gL binding to the R103E^{EphA2} mutant is disrupted, as also seen

358   in the BLI experiments, and/or that binding did not lead to dimer stabilization. These data further

359   corroborate our findings that R103^{EphA2} plays an essential role in gH/gL binding. Here again, we

360   observed an increase in the Intrinsic FRET, which indicates that the fluorescent proteins are in closer

361   proximity, as compared to EphA2 WT in the absence of ligand (Table 1). Similar to the behavior of the

362   E52R^{gH}/gL variant, this effect could be a consequence of R103A^{EphA2} binding to gH/gL, at the high gH/gL

363   concentrations used, that would be transmitted to the EphA2 intracellular domains.

364

365   HHV-8 gH/gL induced EphA2 dimers on cell surface are stabilized via the 'dimerization'

366   interface

367   We showed that when bound to gH/gL, EphA2 is a constitutive dimer. To determine if the

368   EphA2 dimers form via one of the already described interaction surfaces – the dimerization (DIN) or

369 clustering interface (CIN), as reported previously [47] (Fig. S2), we transfected HEK293T cells with the

370 EphA2 variants with perturbed dimerization (G131Y) or clustering (L223R/L254R/V255R) interfaces

371 and treated them with soluble gH/gL ectodomains. The binding of these variants to gH/gL in solution,

372 as measured by BLI, was not affected by the mutations, all of which reside outside of the gH/gL binding

373 site (Fig. S2). The dimerization curves and FRET efficiencies for these mutants in the presence of gH/gL

374 are shown in Fig. 5 and Fig. S8, respectively, with the fit parameters listed in Table 1. We observed a

375 significant decrease in the dimerization due to the $G131Y^{EphA2}$ mutation (Table 1; Fig. 5C), and a small

376 effect due to the $L223R/L254R/V255R^{EphA2}$ mutations (Table 1; Fig. 5D). Thus, $G131^{EphA2}$ plays an

377 important role in the stabilization of EphA2 dimers bound to gH/gL, implying that the EphA2 dimers

378 are formed via DIN. This also supports our finding that gH/gL induces EphA2 dimers and not higher

379 order oligomers, as these oligomers are known to engage both the DIN and the CIN (Fig. S2).

380

381 HHV-8 gH/gL binding to EphA2 expressed on cells induces cell contraction

382   The interactions between Eph receptors and ephrin ligands is known to stimulate cell

383 contraction, a signaling response that plays a role in developmental processes including axon guidance

384 and tissue patterning [65]. To test if the recombinant gH/gL proteins induce similar effects, we performed

385 the assays in HEK293T cells, which express very low amounts of EphA2 (generally below the Western

386 blot detection limit[47]). Therefore, we generated a HEK293T cell line that stably expressed EphA2, and

387 measured cell contraction induced by gH/gL and the $E52R^{gH}$/gL variant that bound weakly to EphA2

388 (Fig. 2D). The EphA2 LBD, alone or precomplexed with gH/gL (gH/gL-LBD) was used as negative control,

389 and dimeric ephrin-A1-Fc as a positive control (described in the MM section). Untransfected HEK293T

390 cells were treated with gH/gL in control experiments. The cells were fixed with paraformaldehyde

391 (PFA), permeabilized, stained for actin and imaged (representative images are displayed in Fig. 6A).

392 Histograms showing the mean cell area measured for each condition show that EphA2-HEK293T cells

393 stimulated with gH/gL were significantly smaller in size compared to every other condition except for

394 cells stimulated with dimeric ephrin-A1-Fc (Fig. 6B). This demonstrates that gH/gL triggered

395 downstream signaling through EphA2, reminiscent to the ephrin-A1 induced signaling. Notably,

396 untransfected HEK293T cells stimulated with gH/gL were also smaller than cells that were not

397 stimulated, but not to the same extent as cells that stably express low levels of EphA2. When

398 stimulated with $E52R^{gH}$/gL, EphA2-HEK293T cells were slightly smaller than untreated cells, but not to

399 the same extent as gH/gL-stimulated cells. The mean cell area determined for EphA2-HEK293T cells in

400 response to $E52R^{gH}$/gL was not statistically different from the area of untransfected HEK293T cells

401 stimulated with gH/gL. Little to no differences in cell area are observed in EphA2-HEK293T cells upon

402 incubation with EphA2 LBD or with the preformed gH/gL-LBD complex.

403   To corroborate our findings in the fixed cells and exclude possible artifacts induced by PFA

404 fixation, we performed a cell contraction assay without fixation using live HEK293T cells transiently

405   transfected with full-length EphA2-eYFP. Soluble recombinant ectodomains of gH/gL, EphA2 LBD, or

406   the gH/gL-LBD complex were added to the media. As in the fixed cell contraction assay, significant live

407   cell area reduction was observed only when free gH/gL was added (Fig. 6C, D). These studies confirm

408   that gH/gL mimics ephrin-A1 binding and signaling through EphA2.

14

Discussion

The structure of the HHV-8 gH/gL complex bound to EphA2 LBD revealed two major gL elements important for binding - the N-terminal segment (res 22-30) and strands β2 and β3, the latter forming a mixed β-sheet with the EphA2 LBD (Fig. 2A). The gL residues form extensive van der Waals contacts and 14 hydrogen bonds with the LBD in total (Table S2A). Sequence alignment of gL from the gammaherpesvirus family shows preference for hydrophobic residues (Ala, Ile, Val) in the N-terminal segment (Fig. S10) consistent with the constraints imposed by packing of these side chains within the 'channel' formed by the hydrophobic residues from the EphA2 and gL β strands ('roof') (Fig. 2). In a cell-cell fusion assay, Su *et al.* reported that gH/gL from other gammaherpesvirus genera, the bovine Alcelaphine gammaherpesvirus 1 (AIHV-1) from the *Macavirus* genus, and Equid gammaherpesvirus 2 (EHV-2) from the *Percavirus* genus, bind to human EphA2 to trigger fusion, and suggested a potential for the spillover of animal herpesviruses to humans [52]. They also demonstrated that this was not the case for the gH/gL from murid herpesvirus 4 (MHV68), which with HHV-8 belongs to the *Rhadinovirus* genus. We performed comparative sequence analyses and found that the N-terminal segment of MHV68 gL contains a number of charged residues (NH_3^+-KILPKHCC...), which could preclude it from fitting into the human EphA2 binding 'channel'. The same is true for gL from another rodent herpesvirus, cricetid gammaherpesvirus 2, whose N-terminus (NH_3^+-IIGSFLARPCC) also contains a charged residue (Fig. S10), and we predict that this gH/gL complex would have weak binding affinity for human EphA2 as well. We therefore propose that the amino acid composition of the N-terminal gL segment can serve as a predictor for the potential for binding to human EphA2, and that the presence of charged or polar amino acids would weaken or abrogate the binding.

The C-terminal gL segment (residues 129-167) was not resolved in the structure, likely because the residues reside within a flexible region that seems to point away from the complex and is not involved in contacts neither with gH nor EphA2. This finding is consistent with the co-immunoprecipitation experiments done with HHV-8 gH co-expressed with the gLΔ135-164 variant, which could still form a complex with gH and EphA2 [66]. This segment is absent from the EBV gL (Fig. S10) indicating a possibly virus-specific function.

Based on a series of BLI measurements we determined the Kd for WT HHV-8 gH/gL and EphA2 ectodomains to be in subnanomolar range. Decreasing the pH to 5.5, the endosomal pH at which the viral and endosomal membranes fuse to release the HHV-8 capsids into the cytoplasm [67], did not affect the Kd (Fig S7A), suggesting that gH/gL dissociation from EphA2 is not required for fusion. This would imply that gH/gL bound to EphA2 could still activate gB, or that there is a fraction of unliganded gH/gL that could interact with gB. The subnanomolar Kd value was obtained when the entire EphA2 ectodomain instead of the LBD alone was used, demonstrating that the EphA2 binding site for gH/gL

15

443   resides in the LBD and that gH/gL does not interact with the downstream EphA2 domains. Higher

444   dissociation constants for HHV-8 gH/gL and EphA2 of 3 or 9nM (depending on the orientation of the

445   molecules) and 16nM were reported by two other groups, respectively [52,60]. The discrepancies might

446   be due to the overestimation of the gH/gL concentration, which was purified via a tag on gH, resulting

447   in the protein preparation that contained gH/gL and free gH [60]. Su *et al.* measured the affinities by SPR

448   with the gH/gL immobilized to the chips by chemical coupling, procedure that modifies the protein

449   surface and thus likely the binding site in a fraction of gH/gL [52]. We designed the experiment to be able

450   to separate the gH/gL complex from free gH by purifying the complex via the affinity tag on gL. The

451   gH/gL was then immobilized to the sensors via the C-terminal affinity tag on gH, which is distal to the

452   EphA2 binding site (Fig. S6). We therefore think that our data represent so far the most accurate

453   quantification of the strength of gH/gL EphA2 interactions. The subnanomolar Kd for the WT proteins

454   were obtained also in an inverted system i.e. when the EphA2 ectodomain or LBD were immobilized

455   via affinity tag on its C-terminus and gH/gL was added as analyte (Fig S7B).

456   The residues of gH implicated in interactions with Eph receptors had been identified previously

457   in a mutagenesis study [66]. In particular, E52^{gH} and F53^{gH} in HHV-8, and the equivalent residues - E54^{gH}

458   and F55^{gH} in rhesus RRV gH - had been found essential for EphA2 binding *in vitro*[24]. These residues are

459   well conserved in gH of gamma-herpesviruses [24]. The recombinant HHV-8 and RRV viruses carrying the

460   mutations in this gH region were still able to attach to cells and infect them, although with one order

461   of magnitude reduction in efficiency, by being re-targeted to other cellular attachment factors and

462   receptors. We noticed that the gH β-turn (SIEL<u>EF</u>NGT) including E52^{gH} and F53^{gH} (underlined), carries

463   resemblance to the motif located within a GH$^{ephrin-A1}$ loop that is the main interaction structural

464   element inserting into the EphA2 cavity (Fig. 3). A conserved glutamic acid residue in the same GH$^{ephrin-}$

465   ^{A1} loop (E119$^{ephrin-A1}$) forms salt bridge with the conserved R103 in the GH^{EphA2} loop (Fig. 3B, Fig. S1),

466   which is the most important residue for ephrin binding, as its mutation to glutamic residue entirely

467   abolished the interaction [43]. In our structure the R103^{EphA2} forms 2 hydrogen bonds and 1 salt bridge

468   with the E52^{gH}, which is substantially less than the gL contribution (14 HB and extensive buried surface

469   area) (Table S2). In EBV gH/gL the equivalent residue E30^{gH} is located away from the EphA2 binding

470   interface due to a different organization of the N-terminal part of gH compared to the HHV-8 gH,

471   possibly contributing to the reported weaker affinity with a Kd in the μM range [52] (the EBV gH and

472   EphA2 in fact do not form any contacts). To determine to what extent the HHV-8 E52^{gH} influences

473   interactions with EphA2, we performed biophysical (gH/gL and EphA2 ectodomains in solution) and

474   cellular assays (EphA2 full-length membrane bound and gH/gL ectodomains in solution). We produced

475   recombinant gH/gL variants carrying the mutations E52R^{gH} or E52A^{gH} and showed that both had

476   reduced binding to EphA2 ectodomains in solution (Fig. 2D). When the cells expressing full-length

477   EphA2 were treated with the recombinant HHV-8 E52R^{gH}/gL, the changes reported for ephrin ligands

478   [68] and induced by the WT gH/gL, such as increased EphA2 dimerization and cell contraction (Fig. 4A,

16

479   Fig. 6), were not observed. Our data therefore demonstrate that the E52^{gH} is an important molecular

480   determinant for EphA2 binding, further highlighting the gH/gL mimicry with ephrin ligands. While the

481   single structural element of ephrins, the GH loop, engages in polar as well as hydrophobic interactions

482   with EphA2, in HHV-8 gH/gL the same contributions are made by E52^{gH} and the N-terminal segment of

483   gL.

484   EphA2 receptors are present on the cell surface in a dynamic monomer-dimer equilibrium,

485   which shifts towards dimers and dimer-made oligomers as a function of ephrin ligand concentration

486   [18,69]. EphA2 signaling oligomers can be stabilized via one of the two opposite interfaces - the DIN and

487   the CIN. In the absence of ligand, the EphA2 dimers are stabilized via CIN [47]. The initial formation of a

488   tetramer – a pair of EphA2 receptor-ligand complexes - is thought to be driven by the ephrins that

489   behave as bivalent ligands interacting with their EphA2 partner molecule through the high-affinity site,

490   and through a secondary site with the other EphA2 molecule from the same tetramer, holding together

491   the whole assembly (Fig. S2). In this arrangement the EphA2 dimers were reported to be stabilized via

492   the GH^{Epha2} loops (DIN), while the larger clusters that form as the ligand concentration increases are

493   formed via contacts between adjacent CRD interfaces (CIN) (Fig. S2) [44,45]. In other words, the

494   association via DIN results in EphA2 dimers, while CIN interactions can result in EphA2 dimers or larger

495   oligomers. (Fig. S2). Our data indicate that once the gH/gL binds, a structural transition is induced and

496   EphA2 dimers are formed via DIN. To explore why EphA2 dimers and not larger oligomers were

497   observed in our experiments, we constructed a model in which unliganded EphA2 ectodomains (PDB

498   2X10) [29] were superimposed onto the EphA2 LBD bound to the gH/gL, preserving the packing of the

499   LBD-gH/gL we observed in the crystal (Fig. S9). This theoretical model reflects the putative

500   arrangement EphA2 receptors expressed on cells would adopt upon binding to gH/gL, and indicates

501   that the CINs would be too far apart to mediate EphA2 clustering, corroborating our 'gH/gL induced

502   EphA2 dimer' finding.

503   The EphA2 dimers we observe in the crystal structure and in FSI-FRET studies, formed via the

504   DIN, would presume ligand-driven stabilization resembling the formation of the Eph-ephrin tetramers

505   described above. Analyses of the contacts in our structure show however the gH/gL molecules do not

506   make contacts with the second EphA2 from the DIN-stabilized tetramer, but rather with an EphA2 from

507   the neighboring EphA2 tetramer (Fig. S9). This poses question of how the gH/gL-induced EphA2 dimers

508   are stabilized, and why CIN-stabilized EphA2 dimers bound to gH/gL are not observed on the cell-

509   surface instead. We analyzed the DINs in unliganded EphA2 receptor and in complex with ephrin

510   ligands and HHV-8 gH/gL. When EphA2 is bound to an ephrin ligand, the DIN is stabilized by increased

511   buried surface area and more hydrogen bonds compared to unliganded EphA2 (Table S3). The values

512   obtained for gH/gL induced EphA2 dimerization (16 HBs and 693 A^2 interface) are comparable to the

513   stabilization of the same interface when bivalent ephrin ligands are bound, indicating that binding of

514   gH/gL to EphA2 LBD stabilizes the DIN sufficiently even though gH/gL does not seem to behave as a

515   bivalent ligand bridging the two EphA2-gH/gL together. Our model would indicate, although this

516   remains speculative, that gH/gL would preferentially bind to the monomeric EphA2 receptors on cells,

517   shifting the equilibrium between the CIN-stabilized, unliganded EphA2 dimers to monomeric EphA2,

518   which once bound to gH/gL would be stabilized via the DIN.

519   Ephrin ligands are expressed on cells as membrane-bound monomers, and Eph receptor

520   clustering and activation at high level are *in vitro* typically induced by addition of soluble dimeric or

521   pre-clustered ephrin ectodomains that mimic their ephrin high concentration when expressed at the

522   cell surface. Ephrin-A1 ligand was also found as a soluble molecule, being released from cancerous

523   cells by cleavage by cellular proteases. Such soluble, monomeric ephrin (m-ephrin) was demonstrated

524   to be a functional ligand, able to activate the EphA2 receptor by inducing tyrosine phosphorylation [70],

525   internalization of EphA2 and cell retraction, overall decreasing the cellular oncogenic potential [71].

526   These beneficial cellular responses are characterized as the outcome of the so-called canonical Eph

527   receptor activation [72]. The structural and functional mimicry of HHV-8 gH/gL and ephrin-A1 would

528   suggest that the HHV-8 interactions with EphA2 trigger canonical signaling pathways, consistent with

529   the observed increased endocytosis and overall EphA2 phosphorylation upon virus binding [20], as well

530   as gH/gL induced cell contraction that we report in Fig. 6. Chen *et al.* reported a different outcome

531   when ephrin-A1 ligands were presented to EphA2-expressing cells in a polarized manner; the Src

532   mediated signaling was activated instead, promoting cell motility and malignancy via phosphorylation

533   of serine and not tyrosine residues (the so-called non-canonical EphA2 activation) [48]. In that light it is

534   interesting that HHV-8 binding to fibroblasts was also reported to result in Src recruitment by androgen

535   receptor, a steroid-activated transcription factor that interacts with the intracellular domain of EphA2.

536   Src activation in this case led to phosphorylation of the S897^{EphA2} in the intracellular EphA2 domain i.e.

537   activation of the non-canonical pathway, which was a prerequisite for HHV-8 infection [73]. These

538   conflicting observations raise the question of what type of signaling HHV-8 gH/gL activates to enter

539   the cells. The canonical and non-canonical pathways were thought to be mutually exclusive, but

540   Barquilla *et al.* recently reported that the two can co-exists and that the EphA2 canonical signaling can

541   be rewired in prostate cancer cells by androgenic receptors leading to the phosphorylation of the same

542   S897^{EphA2} residue [30] implicated in HHV-8 entry [73]. The authors proposed that this EphA2 reprogramming

543   could have implications for the disease progression. It will be important to discern if a similar interplay

544   of the two seemingly antagonistic EphA2 pathways exist in cells infected with HHV-8. It is also possible

545   that there is a temporal regulation and that different EphA2 signaling pathways are activated during

546   the primary infection (canonical, which would stimulate virus internalization via endocytosis) and

547   reactivation (non-canonical, which would increase cellular oncogenic potential).

548   In this report we present the structure of the HHV-8 gH/gL bound to EphA2, and show that the

549   gH/gL induces dimerization of EphA2 expressed by cells as well as morphological changes at cellular

550   level, resembling the action mode of ephrin ligands. It is possible that the membrane anchored gH/gL

551   at the virion surface could induce EphA2 oligomerization into even larger aggregates, in particular if

552   membrane regions with higher local gH/gL concentration exist in virions, emulating the conditions of

553   high ephrin ligand concentration. What is clear however is that at the mechanistic level HHV-8 gH/gL

554   and ephrin ligands induce formation of the same EphA2 dimers, and that these dimers are already

555   functional leading to cytoskeletal rearrangements and cell contraction. How the structural changes

556   that gH/gL binding initiates are transmitted to the EphA2 intracellular domain, and which types of

557   signaling cascades are elicited and when during the virus life cycle are the questions that need to be

558   addressed next.

559

Material and methods

561

Protein expression and purification for crystallization

HHV8 gH/gL: The segments coding the ectodomain of HHV8 gH (residues 26 to 704) and the entire gL (residues 21 – 167) were each cloned from the already described plasmids [20] into the pT350 vector [74] for expression in Schneider S2 *Drosophila* cells (S2 cells). The Cys58 on gL was predicted to be unpaired based on the sequence alignment with EBV gL and was mutated to Ser to prevent potential formation of disulphide-linked dimers. The pT350 vector contains inducible metallothionein promoter activated by divalent cations, the exogenous *Drosophila* Bip signal peptide (MKLCILLAVVAFVGLSLG *RS*), underlined, that drives protein secretion appended to the N-terminus of the protein upstream of the 5' cloning site. The *RS* are vector residues that code for the BglII cloning site. A double strep tag (DST) for affinity purification at the C-terminus was added downstream of the 3' cloning site. The sequence of the DST in our pT350 plasmid is FEDDDDK*AG***WSHPQFEK***GGGSGGGSGGGS***WSHPQFEK**, where DDDDK is the enterokinase cleavage site and the sequences in bold correspond to the two strep tags separated by a GS linker (italics). The residues FE come from the vector *BstBI* cloning site.

HHV-8 gH can be secreted without being bound to gL [75], and the complex purification via a gH tag resulted in a mixture of the gH/gL complex and free gH, which were difficult to separate on size exclusion chromatography (SEC) due to the small size difference (gH has a molecular weight of 75 kDa, and gL 20 kDa). This is why it was crucial for gH/gL purification to add the tag for affinity purification only on gL (Fig. 1A). Thus, the gL was cloned to contain the DST at the C-terminus, and gH has a stop codon before the DST. The resulting expression plasmids were named gH[nt]pT350 and gLC58S[st]pT350, respectively, where 'nt' and 'st' stand for no tag and strep tag, respectively. Such choice was made to allow affinity purification of the gH/gL complex via gL.

It is worth noting that due to the design of the pT350 vector for cloning via restriction digestion the expressed proteins end up having two extra residues RS (*BglII* site) at the N-terminus. The gLC58S[st]pT350 and gH[nt]pT350 both contain the RS before the first authentic residues of the mature gL (Y21) and gH (L26).

The gH[nt]pT350 and gLC58S[st]pT350 plasmids were co-transfected in the S2 cells along with the plasmid encoding puromycin resistance, and the stably transfected cell lines were established by puromycin selection during 3-4 weeks following the previously established protocol [76]. The expression was induced by addition of 0.5mM $CuSO_4$, and the protein was purified from the supernatant 7-10 days post induction. After purification on Streptactin column (IBA Biosciences) and Superdex S200 16/60 GL column (GE life sciences), around 1 milligram of the gH/gL heterodimer was obtained per

593   liter of cell culture (the same amount of the aggregated protein was present). SEC running buffer was

594   10 mM Tris, 50mM NaCl pH 8.0.

595

596   **EphA2 LBD:** The EphA2 gene segment that encodes for residues 23-202 was amplified from the vector

597   [20] and cloned into the pT350 vector for expression in S2 cells (EphA2LBD[st]pT350 construct). The

598   expressed protein contained the DST at the C-terminus. Affinity and SEC purifications were done as

599   described for gH/gL above. Around 10 milligrams of pure EphA2 LBD were obtained from 1 liter of cell

600   culture.

601

602   **Preparation and purification of the trimeric complex EphA2 LBD-HHV8 gH/gL for crystallization:** HHV-

603   8 gH has 14 predicted N-glycosylation sites, gL one and EphA2 LBD none. To increase the probability

604   that the complex would crystallize, the gH/gL complex was enzymatically deglycosylated with

605   recombinant Endoglycosydase D (endo-β-N-acetylglucosaminidase from *Streptococcus pneumoniae*

606   i.e. EndoD [77]), in 100mM sodium-citrate buffer pH 5.0, 150mM NaCl for 18h at 25°C. The ratio of

607   protein to EndoD was 40 to 1 (w:w). To remove the EndoD and exchange the reaction buffer, the

608   deglycosylated complex was purified on Superdex S200 column in 10 mM Tris, 50mM NaCl pH 8.0, and

609   then mixed with the purified EphA2 LBD in 1:1.3 molar ratio (gH/gL : EphA2 LBD). The complex was

610   incubated at 4°C for 1h to over-night, and then re-purified on Superdex S200 to separate the excess

611   EphA2 LBD. The running buffer in all SEC purifications was 10mM Tris pH 8, 50mM NaCl. The trimeric

612   complex was stable on SEC and presence of gH/gL and the EphA2 LBD in the complex peak was verified

613   by SDS-PAGE gel analysis.

614

615   Crystallization

616   The tertiary complex in 10 mM Tris pH 8, 50 mM NaCl was concentrated to 5.1 mg/ml in Vivaspin

617   concentrators with the 10 kDa cut-off. Crystallization screening was performed at the Institut Pasteur

618   Core facility for crystallization [78] by vapor diffusion, in sitting drops of 0.4 μl containing equal volumes

619   of the protein and reservoir solution. The drops were dispensed in 96-well Greiner plates by a

620   Mosquito robot (TTPLabtech, Melbourn, UK) and images were recorder by a Rock-Imager 1000

621   (Formulatrix, Bedford, MA, USA). Initially, crystals were found in numerous conditions, but none

622   diffracted better than 5Å. To improve these crystals, Hampton additive screen HT (HR2-138) was set

623   up next based on one of the initial hits, and crystals grown in 0.1M Na-malonate pH 5, 14.2% PEG 3350

624   in the presence of 14 mM adenosine-5'-triphosphate disodium salt hydrate diffracted to 2.7 Å. These

625   crystals were transferred into the crystallization solution supplemented by 20% ethylene glycol as a

626   cryo-protectant and flash-frozen in liquid nitrogen.

627

628 Data collection and structure determination

629 Data collected at the Proxima 1 beamline at the French national synchrotron facility (SOLEIL, St Aubin,

630 France) were indexed, integrated, scaled and merged using XDS[79] and AIMLESS[80]. Molecular

631 replacement was done with Phaser within Phenix [81][82] using as search models the EphA2 LBD structure

632 (Protein Data Bank [PDB] accession number 3HEI) and the HHV8 gH/gL model that was generated in

633 Phyre2 [55] based on the sequence similarity with the EBV gH/gL (PDB code 3PHF). The partial solution

634 containing EphA2 LBD and parts of gH was obtained, and was extended by iterative rounds of model

635 building (Autobuild [83] in Phenix and manual building in Coot[84]) and refinement using Buster[85] and

636 Phenix [82]. The final model converged to R_{work}/R_{free} of 0.22/0.24. The final map displayed clear electron

637 density for residues 27-200 of EphA2 (with a break in the J helix region (residues 148-162) and GH loop

638 (G111)), residues 21-128 for gL, and residues 35-696 gH with the exception of several short regions of

639 poor density that precluded unambiguous placement of the polypeptide chain (Fig. 1A).

640 The crystallization conditions, crystal parameters, data statistics, and refinement parameters

641 are shown in Table S1. Superpositions of structures and all structural figures were generated with

642 PyMOL (version 1.3r1)[86]. The atomic coordinates and structure factors for trimeric complex EphA2

643 LBD-HHV8 gH/gL have been deposited in the RCSB Protein Data Bank with the PDB code 7B7N.

644

645 Expression of HHV8 gH/gL and EphA2 variants in mammalian cells

646 To avoid lengthy selection of the stably transfected S2 cells expressing recombinant proteins (4-5

647 weeks), a panel of gH/gL and EphA2 variants to be tested in biophysical assays was ordered as synthetic

648 genes (GenScript) cloned in pcDNA3.1 (+) vector for transient expression in mammalian Expi293 cells

649 (5-7 days). The reason mammalian cells were not used for production of the proteins used for

650 crystallizations is that gH/gL complex is heavily glycosylated and the complex sugars added by

651 mammalian cells are typically detrimental for protein crystallization and cannot be enzymatically

652 removed unlike the simple Endo-D and Endo-H sensitive carbohydrates added by insect cells.

653 The mammalian cell expression constructs for gH and gL (residues 21 – 167, and 26-704 respectively)

654 contained at the N-termini an exogenous murine Ig κ-chain leader sequence that targets protein to

655 secretory pathway (Coloma et al., 1992) (METDTLLLWVLLLWVPGSTG). Different affinity tags were

656 added to their C-termini - for gH construct (gH[his]pcDNA3.1) an enterokinase cleavage site (underlined)

657 flanked by two GS linkers (italics) was followed by an octa-his tag (bold) (*GS* DDDDK *SGS* **HHHHHHHH**),

658 and for gL a DST (gL[st]pcDNA3.1; the DST sequence is the same as in the gLC58S[st]pT350 construct

659 described above). The EphA2 variants contained the endogenous signal peptide at the N-terminus and

660 ended at residue 534 followed by a DST tag.

661

662 Biophysical analyses

663   **SEC-MALS measurements:** The complexes were formed by incubating gH^{his}/gLst and EphA2st, both

664   produced in mammalian cells as described above, in 1:1.3 molar ratio for 30 minutes at 4°C ($\sim$100 µg

665   of gH/gL were mixed with 80 µg of EphA2 ectodomains or 30 µg of the EphA2 LBD in PBS in total

666   volume of 200 µl). Assembled complexes were injected into Superdex 200 10/300 GL column (GE life

667   sciences) using 500 µl loop, and run in PBS at a flow rate of 0.4 ml/min. The samples passed through a

668   Wyatt DAWN Heleos II EOS 18-angle laser photometer coupled to a Wyatt Optilab TrEX differential

669   refractive index detector. Data were analyzed with Astra 6 software (Wyatt Technology Corp).

670

671   **Biolayer interferometry measurements:** Biolayer interferometry (BLI) was applied to determine the

672   effect of gH/gL and EphA2 mutations on the complex dissociation constant (Kd). The measurements

673   were carried out on an Octet RED384 instrument (ForteBio). Affinity and SEC purified gH^{his}/gLst

674   produced in mammalian Expi293 cells was immobilized on Ni^{2+}-NTA sensors (ForteBio) in PBS. The

675   loaded and equilibrated biosensors were dipped into analyte solutions containing 250 nM to 1 nM

676   EphA2 variants in PBS containing 0.2 mg/ml BSA (the assay buffer).

677   Association and dissociation were monitored for 250 and 500 seconds respectively. Sensor reference

678   measurement was recorded from a sensor not loaded with gH/gL and dipped in PBS. Sample reference

679   was recorded from a sensor loaded with gH/gL that was dipped in the assay buffer. Specific signals

680   were calculated by double-referencing, that is, subtracting non-specific signals obtained for the sensor

681   and sample references from the signals recorded for the gH/gL-loaded sensors dipped in EphA2 analyte

682   solutions. Association and dissociation profiles, as well as steady-state signal versus concentration

683   curves, were fitted assuming a 1:1 binding model.

684   Cell culture used in FRET and contraction experiments

685   Human embryonic kidney (HEK) 293T cells were purchased from American Type Culture Collection

686   (Manassas, VA; CRL-3216). The cells were cultured at 37 °C and 5% CO$_2$ in Dulbecco's Modified Eagle

687   Medium (DMEM; Thermo Scientific; 31600-034) that contained 3.5 g/L D-glucose, 1.5 g/L sodium

688   bicarbonate, and 10% fetal bovine serum (FBS; Sigma-Aldrich; F4135). The cells were passed up to 25

689   times and then discarded.

690

691   Fixed cell contraction assay

692   HEK293T cells transiently transfected with WT EphA2-eYFP were selected with 1.6 mg/ml G-418

693   solution (Roche; 4727878001) for 12 days to generate a stable cell line. The concentration of G-418

694   was determined using a kill curve. HEK293T cells or EphA2 HEK293T stable cells were seeded (1 x 10^4

695   cells/well) into 8-well tissue culture chambered coverglass slides (Thermo Scientific; 12565338) and

696   cultured for 36 hours. The cells were then washed twice with serum-free, phenol red-free media and

23

697 were serum starved for 12 hours overnight. The cells were washed twice with PBS, followed by

698 treatment for 10 min at 37°C with PBS or 200 nM gH/gL, 200 nM gH E52R/gL, 200 nM LBD, 200 nM

699 gH/gL-LBD, or 0.5 µg/ml ephrin-A1-Fc in PBS. The cells were then fixed in 4% paraformaldehyde in PBS

700 for 15 min at 37°C, permeabilized in 0.1% Triton X-100 in PBS for 15 min 37°C, and incubated with

701 blocking solution (5% FBS, 1% BSA in PBS) for 30 min at room temperature. Then, the cells were stained

702 for actin using rhodamine-conjugated phalloidin (Thermo Fisher Scientific; R415) for 90 min at room

703 temperature. The lyophilized phalloidin-rhodamine powder was reconstituted in DMSO to make a 40x

704 stock solution and then diluted with blocking buffer to make a 1x solution which was added to the

705 fixed cells. The cells were washed twice with PBS in between each step. Finally, starvation media was

706 added to each well prior to imaging. Actin-stained fixed cells were imaged with a Leica TCS SP8 confocal

707 microscope equipped with a HyD hybrid detector and a 63x objective. The measurements were

708 performed with a 552 nm excitation diode laser at 0.5% power using the dsRed setting which measures

709 the fluorescence between wavelengths of 562 and 700 nm. The scanning speed was at 200 Hz, the

710 pixel depth at 12-bits, the zoom factor at 1, and the image size at 1024x1024 pixels. Cell area was

711 determined using the ImageJ software (NIH, Bethesda, MD) by drawing a polygon around the

712 membrane of the cells. Statistical significance was determined by one-way ANOVA followed by a

713 Tukey's test using the GraphPad Prism software.

714 Live cell contraction assay

715 HEK293T cells were seeded, transfected with EphA2 WT-eYFP, and serum-starved overnight in the

716 same manner as described in the FRET section. Ten minutes prior to imaging, the media was replaced

717 with starvation media or starvation media containing 200 nM gH/gL, 200 nM LBD, or 200 nM gH/gL-

718 LBD. Cells were imaged with a Zeiss Axio Observer Inverted two-photon microscope using a 63x

719 objective at a wavelength of 960 nm to excite the eYFP fluorophore. Cell area and statistical

720 significance was determined in the same manner used for the fixed cell contraction assay.

721

722 FSI-FRET measurements and analysis

723 For FRET experiments, the cells were seeded in 35 mm glass bottom collagen-coated petri dishes

724 (MatTek Corporation, MA) at a density of 2×10^5 cells/dish and cultured for 24 hours. The cells were

725 co-transfected with EphA2-mTurquoise (mTURQ, the donor) and EphA2-enhanced yellow fluorescent

726 protein (eYFP, the acceptor) in pcDNA, as described [87,88], using 0.5-2 µg of total DNA and the

727 Lipofectamine 3000 reagent (Invitrogen, CA). In control experiments, cells were transfected with either

728 EphA2-mTURQ or EphA2-eYFP and used for calibration as described [53]. Twelve hours following

729 transfection, the cells were washed twice with serum-free, phenol red-free media and serum-starved

730 in the same media for 12 hours overnight. Immediately before imaging, the starvation media was

24

731 replaced with hypo-osmotic media (10% starvation media, 90% diH2O, 25 mM HEPES) to 'unwrinkle'

732 the highly ruffled cell membrane under reversible conditions as described [89]. The soluble proteins were

733 premixed with the hypo-osmotic media before adding to the cells. Cells were incubated for 10 minutes

734 and then imaged under these conditions for approximately 1 hour.

735 Spectral images of HEK293T cells under reversible osmotic conditions were obtained following

736 published protocols [53] with a spectrally resolved two-photon microscope (Zeiss Inverted Axio Observer)

737 equipped with line-scanning capabilities (OptiMis True Line Spectral Imaging system, Aurora Spectral

738 Technologies, WI) [90]. Fluorophores were excited by a mode-locked laser (MaiTai™, Spectra-Physics,

739 Santa Clara, CA) that generates femtosecond pulses between wavelengths 690 nm to 1040 nm. Two

740 images were collected for each cell: one at 840 nm to excite the donor and a second one at 960 nm to

741 primarily excite the acceptor. Solutions of purified soluble fluorescent proteins (mTURQ and eYFP) at

742 known concentrations were produced following a published protocol [91] and imaged at each of these

743 excitation wavelengths. A linear fit generated from the pixel-level intensities of the solution standards

744 was used to calibrate the effective three-dimensional protein concentration which can be converted

745 into two-dimensional membrane protein concentrations in the cell membrane as described [53]. The

746 calibration curve along with the cell images were used to calculate the FRET efficiency and the

747 concentration of donors and acceptors present in the cell membrane [53]. Regions of the cell membrane

748 not in contact with neighboring cells were selected and analyzed to avoid interactions with proteins

749 on adjacent cells.

750 The measured FRET efficiencies (E_{app}) were corrected for 'proximity FRET' (E_{prox}) as described previously

751 [92]. The proximity FRET accounts for donor-tagged molecules and acceptor-tagged molecules coming

752 into close enough proximity to observe a FRET signal (within 100 Å) but not interacting directly. The

753 corrected FRET due to specific interactions between the labeled proteins is given by:

754
$$FRET = \frac{E_{prox} - E_{app}}{2E_{prox} - E_{prox}E_{app} - 1} \qquad (1)$$

755 The corrected FRET depends on the fraction of membrane protein dimers, f_D, and on the acceptor

756 fraction, x_A, according to:

757
$$FRET = f_D x_A \tilde{E} \qquad (2)$$

758 The 'Intrinsic FRET' ($\tilde{E}$) is a structural parameter that depends on the distance between and orientation

759 of the two fluorophores in the dimer but is not dependent on the dimerization propensity [92-94].

760 When the dimeric fraction is 100% (f_D = 1), the corrected FRET does not depend on the concentration

761 of the labeled proteins and thus equation (2) can be simplified further:

762
$$FRET = x_A \tilde{E}. \qquad (3)$$

763 The dependence of the Intrinsic FRET on the distance between the fluorescent proteins in the dimer,

764 d, is given by [93]:

$$\tilde{E} = \frac{1}{1+\left(\frac{d}{R_0}\right)^6} \tag{4}$$

766 where R_0 is the Forster radius for the mTurquoise-eYFP FRET pair, 54.5 Å. Since the fluorescent proteins

767 are attached to the C-terminus of the membrane proteins via long flexible linkers, we assume free

768 rotation of the fluorescent proteins.

769 By rearranging equation (2), the dimeric fraction, f_D, can be determined from the corrected FRET

770 efficiencies and concentrations according to:

$$f_D = \frac{FRET}{x_A \tilde{E}} \tag{5}$$

772 In the case of dimers, the following equation is used to determine the two unknowns K_{diss} and $\tilde{E}$ as

773 described previously [53]:

$$\frac{FRET}{x_A} = \frac{1}{[R_{total}]}\left([R_{total}] - \frac{K_{diss}}{4}\left(\sqrt{1+8[R_{total}]/K_{diss}} - 1\right)\right)\tilde{E} \tag{6}$$

775

776 Fluorescence intensity fluctuations (FIF) spectroscopy measurements and analysis

777 HEK293T cells were seeded as described in the FRET section at a density of 4×10^5 cells/dish. The cells

778 were transiently transfected 24 hours later with 1 μg of EphA2-eYFP using Lipofectamine 3000 and

779 then washed and serum starved twelve hours later. The starvation media was replaced with a 75%

780 hypo-osmotic media (25% starvation media, 75% diH2O, 25 mM HEPES) containing 200 nM gH/gL prior

781 to imaging. A TCS SP8 confocal microscope (Leica) using the photon counting capabilities of the HyD

782 hybrid detector was used to collect images of the cell basolateral membranes. The measurements

783 were performed with a 488 nm excitation diode laser and the emission spectra of YFP were collected

784 from 520-580 nm. The scanning speed was at 20Hz, the pixel depth at 12-bits, the zoom factor at 2,

785 and the image size at 1024x1024.

786 The cell images were analyzed using the FIF software described in [61]. The software performed

787 segmentation of the basolateral membrane into 15x15 pixel regions of interest. Each cell is outlined

788 by researcher prior to segmentation. The segmented data was analyzed using the brightness and

789 concentration calculator in the FIF software [61]. The molecular brightness, ε, was calculated according

790 to:

$$\varepsilon = \frac{\sigma^2 - \sigma_D^2}{<I>} \tag{7}$$

792   where σ^2 is the variance of fluorescence across segments, σ_D^2 is the variance of the noise of the

793   detector, and $< I >$ is the average fluorescence intensity. For a photon-counting detector as used

794   here, the brightness is [64,95]:

795 $$\varepsilon = \frac{\sigma^2}{<I>} - 1 \qquad\qquad (8)$$

796   The brightness values, calculated for thousands of regions of interest, were potted as histograms.

REFERENCES

1   Pellett, P. E. & Roizman, B. in *Fields Virology* Vol. 2 (eds D.M. Knip & P.M. Howley) Ch. 59, 1802-1823 (Lippincott Williams & Wilkins, 2013).

2   Kaposi, M. Idiopathisches multiples Pigmentsarkom der Haut. *Archive für Dermatologieund Syphillis* **4**, 265-173 (1872).

3   Board, P. A. T. E. Kaposi Sarcoma Treatment (PDQ(R)): Health Professional Version. (National Cancer Institute, Bethesda (MD), 2018).

4   Centers for Disease, C. Update on acquired immune deficiency syndrome (AIDS)--United States. *MMWR Morb Mortal Wkly Rep* **31**, 507-508, 513-504 (1982).

5   Beral, V., Peterman, T. A., Berkelman, R. L. & Jaffe, H. W. Kaposi's sarcoma among persons with AIDS: a sexually transmitted infection? *Lancet* **335**, 123-128, doi:10.1016/0140-6736(90)90001-I (1990).

6   Mesri, E. A., Cesarman, E. & Boshoff, C. Kaposi's sarcoma and its associated herpesvirus. *Nat Rev Cancer* **10**, 707-719, doi:10.1038/nrc2888 (2010).

7   Mohl, B. S., Chen, J. & Longnecker, R. Gammaherpesvirus entry and fusion: A tale how two human pathogenic viruses enter their host cells. *Adv Virus Res* **104**, 313-343, doi:10.1016/bs.aivir.2019.05.006 (2019).

8   Veettil, M. V., Bandyopadhyay, C., Dutta, D. & Chandran, B. Interaction of KSHV with host cell surface receptors and cell entry. *Viruses* **6**, 4024-4046, doi:10.3390/v6104024 (2014).

9   Dollery, S. J. Towards Understanding KSHV Fusion and Entry. *Viruses-Basel* **11**, doi:ARTN 1073 10.3390/v11111073 (2019).

10   Connolly, S. A., Jardetzky, T. S. & Longnecker, R. The structural basis of herpesvirus entry. *Nat Rev Microbiol*, doi:10.1038/s41579-020-00448-w (2020).

11   Dollery, S. J. Towards Understanding KSHV Fusion and Entry. *Viruses* **11**, doi:10.3390/v11111073 (2019).

12   Xing, Y. *et al.* A site of varicella-zoster virus vulnerability identified by structural studies of neutralizing antibodies bound to the glycoprotein complex gHgL. *Proc Natl Acad Sci U S A* **112**, 6056-6061, doi:10.1073/pnas.1501176112 (2015).

13   Ciferri, C. *et al.* Structural and biochemical studies of HCMV gH/gL/gO and Pentamer reveal mutually exclusive cell entry complexes. *Proc Natl Acad Sci U S A* **112**, 1767-1772, doi:10.1073/pnas.1424818112 (2015).

14   Chowdary, T. K. *et al.* Crystal structure of the conserved herpesvirus fusion regulator complex gH-gL. *Nat Struct Mol Biol* **17**, 882-888, doi:10.1038/nsmb.1837 nsmb.1837 [pii] (2010).

15   Matsuura, H., Kirschner, A. N., Longnecker, R. & Jardetzky, T. S. Crystal structure of the Epstein-Barr virus (EBV) glycoprotein H/glycoprotein L (gH/gL) complex. *Proc Natl Acad Sci U S A* **107**, 22641-22646, doi:10.1073/pnas.1011806108 1011806108 [pii] (2010).

16   Sathiyamoorthy, K., Chen, J., Longnecker, R. & Jardetzky, T. S. The COMPLEXity in herpesvirus entry. *Curr Opin Virol* **24**, 97-104, doi:10.1016/j.coviro.2017.04.006 (2017).

17   Unified nomenclature for Eph family receptors and their ligands, the ephrins. Eph Nomenclature Committee. *Cell* **90**, 403-404, doi:10.1016/s0092-8674(00)80500-0 (1997).

18   Himanen, J. P. Ectodomain structures of Eph receptors. *Semin Cell Dev Biol* **23**, 35-42, doi:10.1016/j.semcdb.2011.10.025 (2012).

19   Himanen, J. P., Saha, N. & Nikolov, D. B. Cell-cell signaling via Eph receptors and ephrins. *Curr Opin Cell Biol* **19**, 534-542, doi:10.1016/j.ceb.2007.08.004 (2007).

20   Hahn, A. S. *et al.* The ephrin receptor tyrosine kinase A2 is a cellular receptor for Kaposi's sarcoma-associated herpesvirus. *Nat Med* **18**, 961-966, doi:10.1038/nm.2805 nm.2805 [pii] (2012).

21   Chen, J., Zhang, X., Schaller, S., Jardetzky, T. S. & Longnecker, R. Ephrin Receptor A4 is a New Kaposi's Sarcoma-Associated Herpesvirus Virus Entry Receptor. *MBio* **10**, doi:10.1128/mBio.02892-18 (2019).

849 22   Grosskopf, A. K. *et al.* EphA7 Functions as Receptor on BJAB Cells for Cell-to-Cell Transmission
850   of the Kaposi's Sarcoma-Associated Herpesvirus and for Cell-Free Infection by the Related
851   Rhesus Monkey Rhadinovirus. *J Virol* **93**, doi:10.1128/JVI.00064-19 (2019).
852 23   Chen, J. *et al.* Ephrin receptor A2 is a functional entry receptor for Epstein-Barr virus. *Nat*
853   *Microbiol* **3**, 172-180, doi:10.1038/s41564-017-0081-7 (2018).
854 24   Hahn, A. S. & Desrosiers, R. C. Rhesus monkey rhadinovirus uses eph family receptors for entry
855   into B cells and endothelial cells but not fibroblasts. *PLoS Pathog* **9**, e1003360,
856   doi:10.1371/journal.ppat.1003360 (2013).
857 25   Lupberger, J. *et al.* EGFR and EphA2 are host factors for hepatitis C virus entry and possible
858   targets for antiviral therapy. *Nat Med* **17**, 589-595, doi:10.1038/nm.2341
859 nm.2341 [pii] (2011).
860 26   Subbarayal, P. *et al.* EphrinA2 receptor (EphA2) is an invasion and intracellular signaling
861   receptor for Chlamydia trachomatis. *PLoS Pathog* **11**, e1004846,
862   doi:10.1371/journal.ppat.1004846 (2015).
863 27   Aaron, P. A., Jamklang, M., Uhrig, J. P. & Gelli, A. The blood-brain barrier internalises
864   Cryptococcus neoformans via the EphA2-tyrosine kinase receptor. *Cell Microbiol* **20**,
865   doi:10.1111/cmi.12811 (2018).
866 28   Kaushansky, A. *et al.* Malaria parasites target the hepatocyte receptor EphA2 for successful
867   host infection. *Science* **350**, 1089-1092, doi:10.1126/science.aad3318 (2015).
868 29   Kania, A. & Klein, R. Mechanisms of ephrin-Eph signalling in development, physiology and
869   disease. *Nat Rev Mol Cell Biol* **17**, 240-256, doi:10.1038/nrm.2015.16 (2016).
870 30   Barquilla, A. *et al.* Protein kinase A can block EphA2 receptor-mediated cell repulsion by
871   increasing EphA2 S897 phosphorylation. *Mol Biol Cell* **27**, 2757-2770, doi:10.1091/mbc.E16-
872   01-0048 (2016).
873 31   Miao, H., Burnett, E., Kinch, M., Simon, E. & Wang, B. Activation of EphA2 kinase suppresses
874   integrin function and causes focal-adhesion-kinase dephosphorylation. *Nat Cell Biol* **2**, 62-69,
875   doi:10.1038/35000008 (2000).
876 32   Huang, X., Wu, D., Jin, H., Stupack, D. & Wang, J. Y. Induction of cell retraction by the combined
877   actions of Abl-CrkII and Rho-ROCK1 signaling. *J Cell Biol* **183**, 711-723,
878   doi:10.1083/jcb.200801192 (2008).
879 33   Astin, J. W. *et al.* Competition amongst Eph receptors regulates contact inhibition of
880   locomotion and invasiveness in prostate cancer cells. *Nat Cell Biol* **12**, 1194-1204,
881   doi:10.1038/ncb2122 (2010).
882 34   Pitulescu, M. E. & Adams, R. H. Eph/ephrin molecules--a hub for signaling and endocytosis.
883   *Genes Dev* **24**, 2480-2492, doi:10.1101/gad.1973910 (2010).
884 35   Saha, N., Robev, D., Mason, E. O., Himanen, J. P. & Nikolov, D. B. Therapeutic potential of
885   targeting the Eph/ephrin signaling complex. *Int J Biochem Cell Biol* **105**, 123-133,
886   doi:10.1016/j.biocel.2018.10.006 (2018).
887 36   Barquilla, A. & Pasquale, E. B. Eph receptors and ephrins: therapeutic opportunities. *Annu Rev*
888   *Pharmacol Toxicol* **55**, 465-487, doi:10.1146/annurev-pharmtox-011112-140226 (2015).
889 37   Kumar, B. & Chandran, B. KSHV Entry and Trafficking in Target Cells-Hijacking of Cell Signal
890   Pathways, Actin and Membrane Dynamics. *Viruses* **8**, doi:10.3390/v8110305 (2016).
891 38   Holland, S. J. *et al.* Bidirectional signalling through the EPH-family receptor Nuk and its
892   transmembrane ligands. *Nature* **383**, 722-725, doi:10.1038/383722a0 (1996).
893 39   Himanen, J. P., Henkemeyer, M. & Nikolov, D. B. Crystal structure of the ligand-binding domain
894   of the receptor tyrosine kinase EphB2. *Nature* **396**, 486-491, doi:10.1038/24904 (1998).
895 40   Bowden, T. A. *et al.* Structural Plasticity of Eph-Receptor A4 Facilitates Cross-Class Ephrin
896   Signaling. *Structure* **17**, 1679, doi:10.1016/j.str.2009.11.004 (2009).
897 41   Toth, J. *et al.* Crystal structure of an ephrin ectodomain. *Dev Cell* **1**, 83-92, doi:10.1016/s1534-
898   5807(01)00002-8 (2001).
899 42   Himanen, J. P. *et al.* Crystal structure of an Eph receptor-ephrin complex. *Nature* **414**, 933-938,
900   doi:10.1038/414933a
901 414933a [pii] (2001).

902   43   Himanen, J. P. *et al.* Ligand recognition by A-class Eph receptors: crystal structures of the
903   EphA2 ligand-binding domain and the EphA2/ephrin-A1 complex. *EMBO Rep* **10**, 722-728,
904   doi:10.1038/embor.2009.91 (2009).
905   44   Seiradake, E., Harlos, K., Sutton, G., Aricescu, A. R. & Jones, E. Y. An extracellular steric seeding
906   mechanism for Eph-ephrin signaling platform assembly. *Nat Struct Mol Biol* **17**, 398-402,
907   doi:10.1038/nsmb.1782 (2010).
908   45   Himanen, J. P. *et al.* Architecture of Eph receptor clusters. *Proc Natl Acad Sci U S A* **107**, 10860-
909   10865, doi:10.1073/pnas.1004148107
910   1004148107 [pii] (2010).
911   46   Nikolov, D. B., Xu, K. & Himanen, J. P. Eph/ephrin recognition and the role of Eph/ephrin
912   clusters in signaling initiation. *Biochim Biophys Acta* **1834**, 2160-2165,
913   doi:10.1016/j.bbapap.2013.04.020 (2013).
914   47   Singh, D. R., Kanvinde, P., King, C., Pasquale, E. B. & Hristova, K. The EphA2 receptor is activated
915   through induction of distinct, ligand-dependent oligomeric structures. *Commun Biol* **1**, 15,
916   doi:10.1038/s42003-018-0017-7 (2018).
917   48   Chen, Z. *et al.* Spatially modulated ephrinA1:EphA2 signaling increases local contractility and
918   global focal adhesion dynamics to promote cell motility. *Proc Natl Acad Sci U S A* **115**, E5696-
919   E5705, doi:10.1073/pnas.1719961115 (2018).
920   49   Singh, D. R., Pasquale, E. B. & Hristova, K. A small peptide promotes EphA2 kinase-dependent
921   signaling by stabilizing EphA2 dimers. *Biochim Biophys Acta* **1860**, 1922-1928,
922   doi:10.1016/j.bbagen.2016.06.004 (2016).
923   50   Ojosnegros, S. *et al.* Eph-ephrin signaling modulated by polymerization and condensation of
924   receptors. *Proc Natl Acad Sci U S A* **114**, 13188-13193, doi:10.1073/pnas.1713564114 (2017).
925   51   Gomez-Soler, M. *et al.* Engineering nanomolar peptide ligands that differentially modulate
926   EphA2 receptor signaling. *J. Biol. Chem.* **294**, 8791-8805, doi:10.1074/jbc.RA119.008213
927   (2019).
928   52   Su, C. *et al.* Molecular basis of EphA2 recognition by gHgL from gammaherpesviruses. *Nat
929   Commun* **11**, 5964, doi:10.1038/s41467-020-19617-9 (2020).
930   53   King, C., Stoneman, M., Raicu, V. & Hristova, K. Fully quantified spectral imaging reveals in vivo
931   membrane protein interactions. *Integr Biol (Camb)* **8**, 216-229, doi:10.1039/c5ib00202h
932   (2016).
933   54   Sahin, E. & Roberts, C. J. Size-exclusion chromatography with multi-angle light scattering for
934   elucidating protein aggregation mechanisms. *Methods Mol Biol* **899**, 403-423,
935   doi:10.1007/978-1-61779-921-1_25 (2012).
936   55   Kelley, L. A., Mezulis, S., Yates, C. M., Wass, M. N. & Sternberg, M. J. The Phyre2 web portal for
937   protein modeling, prediction and analysis. *Nat Protoc* **10**, 845-858,
938   doi:10.1038/nprot.2015.053 (2015).
939   56   Meszaros, B., Erdos, G. & Dosztanyi, Z. IUPred2A: context-dependent prediction of protein
940   disorder as a function of redox state and protein binding. *Nucleic Acids Res* **46**, W329-W337,
941   doi:10.1093/nar/gky384 (2018).
942   57   Erdos, G. & Dosztanyi, Z. Analyzing Protein Disorder with IUPred2A. *Curr Protoc Bioinformatics*
943   **70**, e99, doi:10.1002/cpbi.99 (2020).
944   58   Backovic, M. *et al.* Structure of a core fragment of glycoprotein H from pseudorabies virus in
945   complex with antibody. *Proc. Natl. Acad. Sci. U.S.A.* **107**, 22635-22640,
946   doi:10.1073/pnas.1011507107 (2010).
947   59   Vleck, S. E. *et al.* Structure-function analysis of varicella-zoster virus glycoprotein H identifies
948   domain-specific roles for fusion and skin tropism. *Proc Natl Acad Sci U S A* **108**, 18412-18417,
949   doi:10.1073/pnas.1111333108 (2011).
950   60   Hahn, A. S. & Desrosiers, R. C. Binding of the Kaposi's sarcoma-associated herpesvirus to the
951   ephrin binding surface of the EphA2 receptor and its inhibition by a small molecule. *J Virol* **88**,
952   8724-8734, doi:10.1128/JVI.01392-14 (2014).
953   61   Stoneman, M. R. *et al.* A general method to quantify ligand-driven oligomerization from
954   fluorescence-based images. *Nat Methods* **16**, 493-496, doi:10.1038/s41592-019-0408-9
955   (2019).

956 62   Adamkova, L. *et al.* Oligomeric Architecture of Mouse Activating Nkrp1 Receptors on Living
957   Cells. *Int J Mol Sci* **20**, doi:10.3390/ijms20081884 (2019).
958 63   Singh, D. R., Ahmed, F., Sarabipour, S. & Hristova, K. Intracellular Domain Contacts Contribute
959   to Ecadherin Constitutive Dimerization in the Plasma Membrane. *J Mol Biol* **429**, 2231-2245,
960   doi:10.1016/j.jmb.2017.05.020 (2017).
961 64   Ahmed, F., Zapata-Mercado, E., Rahman, S. & Hristova, K. The Biased Ligands NGF and NT-3
962   Differentially Stabilize Trk-A Dimers. *Biophys J* **120**, 55-63, doi:10.1016/j.bpj.2020.11.2262
963   (2021).
964 65   Pasquale, E. B. Eph receptor signalling casts a wide net on cell behaviour. *Nat Rev Mol Cell Biol*
965   **6**, 462-475, doi:10.1038/nrm1662 (2005).
966 66   Grosskopf, A. K. *et al.* A conserved Eph family receptor-binding motif on the gH/gL complex of
967   Kaposi's sarcoma-associated herpesvirus and rhesus monkey rhadinovirus. *PLoS Pathog* **14**,
968   e1006912, doi:10.1371/journal.ppat.1006912 (2018).
969 67   Akula, S. M. *et al.* Kaposi's sarcoma-associated herpesvirus (human herpesvirus 8) infection of
970   human fibroblast cells occurs through endocytosis. *J Virol* **77**, 7978-7990,
971   doi:10.1128/jvi.77.14.7978-7990.2003 (2003).
972 68   Himanen, J. P. *et al.* Repelling class discrimination: ephrin-A5 binds to and activates EphB2
973   receptor signaling. *Nat Neurosci* **7**, 501-509, doi:10.1038/nn1237 (2004).
974 69   Nikolov, D. B., Xu, K. & Himanen, J. P. Homotypic receptor-receptor interactions regulating Eph
975   signaling. *Cell adhesion & migration* **8**, 360-365, doi:10.4161/19336918.2014.971684 (2014).
976 70   Wykosky, J. *et al.* Soluble monomeric EphrinA1 is released from tumor cells and is a functional
977   ligand for the EphA2 receptor. *Oncogene* **27**, 7260-7273, doi:10.1038/onc.2008.328 (2008).
978 71   Beauchamp, A. & Debinski, W. Ephs and ephrins in cancer: ephrin-A1 signalling. *Semin Cell Dev*
979   *Biol* **23**, 109-115, doi:10.1016/j.semcdb.2011.10.019 (2012).
980 72   Miao, H. *et al.* EphA2 mediates ligand-dependent inhibition and ligand-independent
981   promotion of cell migration and invasion via a reciprocal regulatory loop with Akt. *Cancer Cell*
982   **16**, 9-20, doi:10.1016/j.ccr.2009.04.009 (2009).
983 73   Wang, X. *et al.* Male hormones activate EphA2 to facilitate Kaposi's sarcoma-associated
984   herpesvirus infection: Implications for gender disparity in Kaposi's sarcoma. *PLoS Pathog* **13**,
985   e1006580, doi:10.1371/journal.ppat.1006580 (2017).
986 74   Krey, T. *et al.* The disulfide bonds in glycoprotein E2 of hepatitis C virus reveal the tertiary
987   organization of the molecule. *PLoS Pathog* **6**, e1000762 (2010).
988 75   Hahn, A. *et al.* Kaposi's sarcoma-associated herpesvirus gH/gL: glycoprotein export and
989   interaction with cellular receptors. *J Virol* **83**, 396-407, doi:10.1128/JVI.01170-08 (2009).
990 76   Backovic, M. & Krey, T. Stable Drosophila Cell Lines: An Alternative Approach to Exogenous
991   Protein Expression. *Methods Mol. Biol.* **1350**, 349-358, doi:10.1007/978-1-4939-3043-2_17
992   (2016).
993 77   Fan, S. Q., Huang, W. & Wang, L. X. Remarkable transglycosylation activity of glycosynthase
994   mutants of endo-D, an endo-beta-N-acetylglucosaminidase from Streptococcus pneumoniae.
995   *J Biol Chem* **287**, 11272-11281, doi:10.1074/jbc.M112.340497 (2012).
996 78   Weber, P. *et al.* High-Throughput Crystallization Pipeline at the Crystallography Core Facility of
997   the Institut Pasteur. *Molecules* **24**, doi:10.3390/molecules24244451 (2019).
998 79   Kabsch, W. XDS. *Acta Crystallogr D Biol Crystallogr* **66**, 125-132 (2010).
999 80   The CCP4 suite: programs for protein crystallography. *Acta Crystallogr D Biol Crystallogr* **50**,
1000   760-763 (1994).
1001 81   Adams, P. D. *et al.* PHENIX: a comprehensive Python-based system for macromolecular
1002   structure solution. *Acta Crystallogr D Biol Crystallogr* **66**, 213-221,
1003   doi:10.1107/S0907444909052925 (2010).
1004 82   Liebschner, D. *et al.* Macromolecular structure determination using X-rays, neutrons and
1005   electrons: recent developments in Phenix. *Acta Crystallogr D Struct Biol* **75**, 861-877,
1006   doi:10.1107/S2059798319011471 (2019).
1007 83   Terwilliger, T. C. *et al.* Iterative model building, structure refinement and density modification
1008   with the PHENIX AutoBuild wizard. *Acta Crystallogr D Biol Crystallogr* **64**, 61-69,
1009   doi:10.1107/S090744490705024X (2008).

1010 84   Emsley, P. & Cowtan, K. Coot: model-building tools for molecular graphics. *Acta Crystallogr D*
1011   *Biol Crystallogr* **60**, 2126-2132 (2004).
1012 85   BUSTER v. 2.8.0 (Global Phasing Ltd., Cambridge, United Kingdom, 2009).
1013 86   The PyMOL Molecular Graphics System (DeLano Scientific, San Carlos, CA, USA, 2002).
1014 87   Singh, D. R. *et al.* EphA2 Receptor Unliganded Dimers Suppress EphA2 Pro-tumorigenic
1015   Signaling. *J Biol Chem* **290**, 27271-27279, doi:10.1074/jbc.M115.676866 (2015).
1016 88   Singh, D. R., Kanvinde, P., King, C., Pasquale, E. B. & Hristova, K. The EphA2 receptor is activated
1017   through induction of distinct, ligand-dependent oligomeric structures. *Commun Biol* **1**, 15,
1018   doi:10.1038/s42003-018-0017-7 (2018).
1019 89   Sinha, B. *et al.* Cells respond to mechanical stress by rapid disassembly of caveolae. *Cell* **144**,
1020   402-413, doi:10.1016/j.cell.2010.12.031 (2011).
1021 90   Biener, G. *et al.* Development and experimental testing of an optical micro-spectroscopic
1022   technique incorporating true line-scan excitation. *Int J Mol Sci* **15**, 261-276,
1023   doi:10.3390/ijms15010261 (2013).
1024 91   Sarabipour, S., King, C. & Hristova, K. Uninduced high-yield bacterial expression of fluorescent
1025   proteins. *Anal Biochem* **449**, 155-157, doi:10.1016/j.ab.2013.12.027 (2014).
1026 92   King, C., Raiu, V. & Hristova, K. Understanding the FRET Signatures of Interacting Membrane
1027   Proteins. *J Biol Chem* **292**, 5291-5310, doi:10.1074/jbc.M116.764282 (2017).
1028 93   Chen, L., Novicky, L., Merzlyakov, M., Hristov, T. & Hristova, K. Measuring the energetics of
1029   membrane protein dimerization in mammalian membranes. *J Am Chem Soc* **132**, 3628-3635,
1030   doi:10.1021/ja910692u (2010).
1031 94   Sarabipour, S., Del Piccolo, N. & Hristova, K. Characterization of membrane protein
1032   interactions in plasma membrane derived vesicles with quantitative imaging Forster
1033   resonance energy transfer. *Acc Chem Res* **48**, 2262-2269, doi:10.1021/acs.accounts.5b00238
1034   (2015).
1035 95   Fox, M. *Quantum optics: an introduction*. Vol. 15 (Oxford Univeristy Press, 2006).
1036

Acknowledgements

Contributions

Conceived and designed the experiments (MB, KH, FR), produced reagents (MB, DB, AH), collected the data (MB, PGC, TL), performed the data analyses (TL, PGC, RP, KH, MB), wrote the paper (MB, KH, TL, FR, PGC, RP, AH, FN).

Figures and figure legends

1050

Table of Contents

1061

1062

1063

1064 Table 1: Summary of the dimerization models fit to FRET data

1065

EphA2 construct	Soluble protein	K_{diss} (receptors/µm²)	Intrinsic FRET, $\tilde{E}$	distance, d (Å)
WT	-	302 ± 68	0.53 ± 0.02	53.6 ± 0.7
WT	gH/gL	100% dimer	0.31 ± 0.01	62.3 ± 0.2
WT	LBD	348 ± 130	0.50 ± 0.03	54.6 ± 1.2
WT	gH/gL-LBD	233 ± 103	0.55 ± 0.03	52.7 ± 1.2
WT	gH E52R/gL	300 ± 71	0.66 ± 0.03	48.9 ± 1.0
R103E	gH/gL	310 ± 124	0.76 ± 0.03	45.0 ± 1.5
G131Y	gH/gL	251 ± 103	0.58 ± 0.03	51.4 ± 1.2
L223R/L254R/V255R	gH/gL	17 ± 12	0.43 ± 0.02	57.1 ± 0.5

1066

1067 Summary of the best-fit values for the dissociation constant (K_{diss}), the structural parameter Intrinsic
1068 FRET ($\tilde{E}$), and the distance between fluorophores (d), obtained by fitting dimerization models to the
1069 FRET data. K_{diss} and $\tilde{E}$ are determined by a two-parameter fit using equation (6) and the distance d is
1070 calculated using equation (4).

1071

Figure 1: Schematic representation of HHV-8 gH, gL and EphA2 and structure of the gH/gL-EphA2 LBD complex
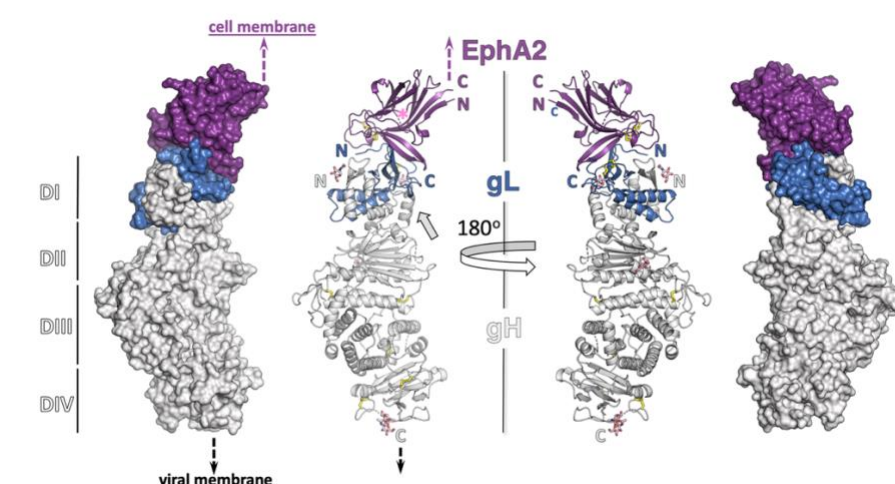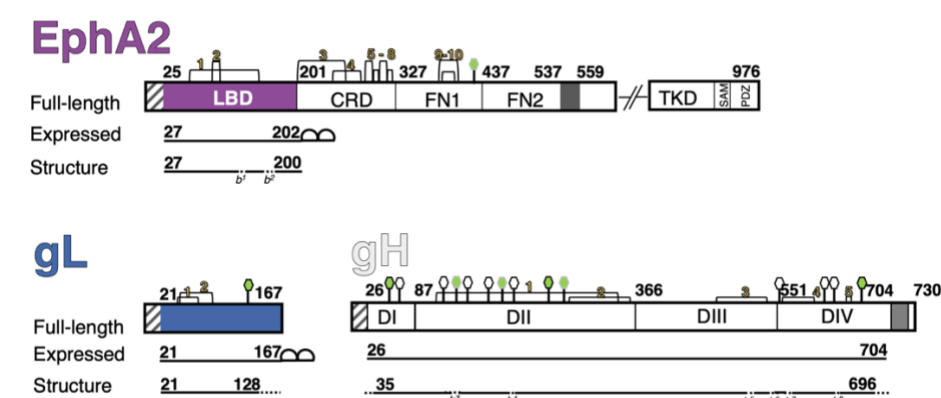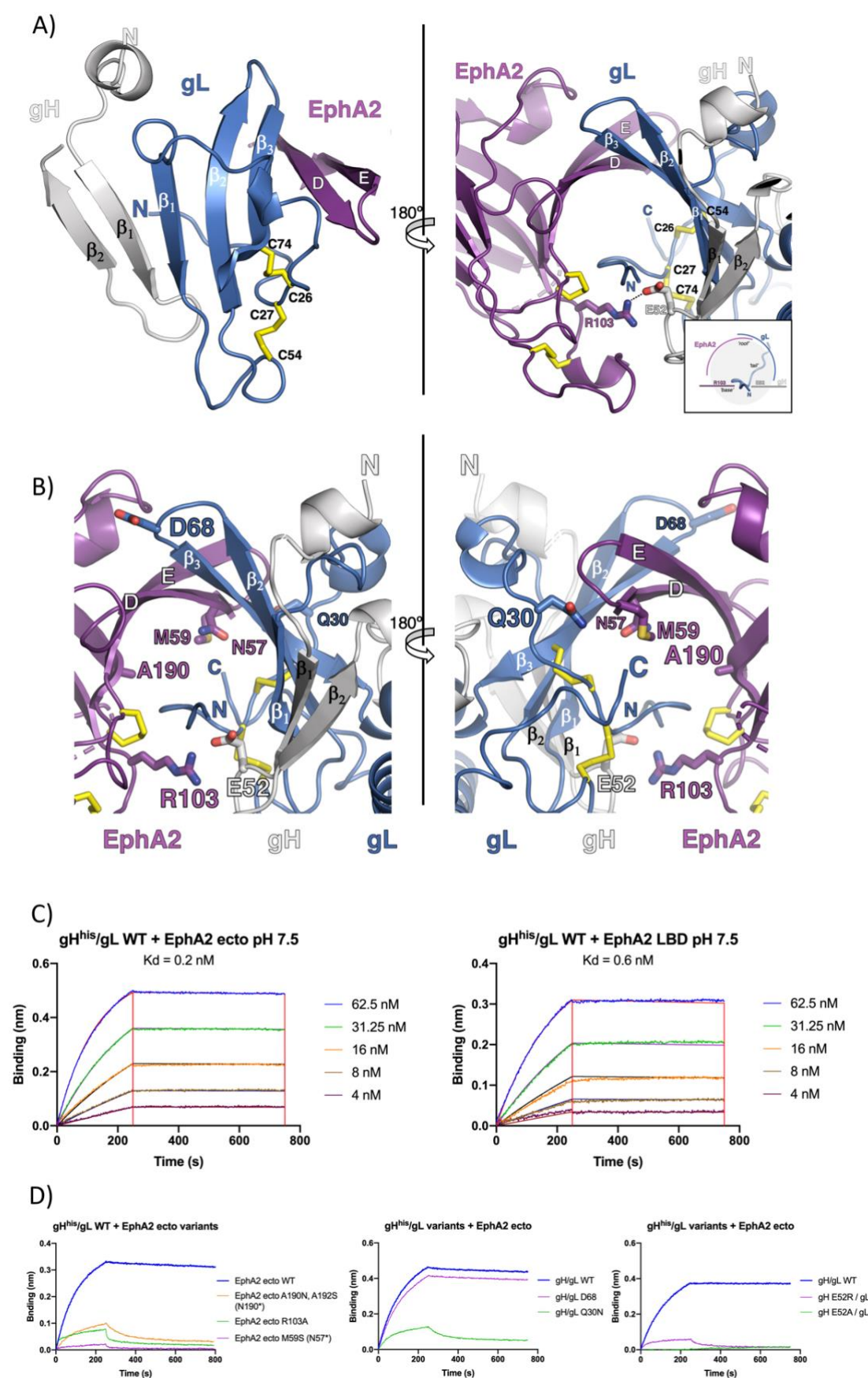

Figure 1 legend

A) Schematic representation of the EphA2 receptor, HHV-8 gL and gH, highlighting the protein segments that were expressed as recombinant proteins for crystallization, and the residues resolved in the structure. The short fragments that could not be built in EphA2 LBD and gH because of the poor electron density are marked with dotted lines and labeled as breaks (*b*) corresponding to the missing residues: b^1 (111), b^2 (148-162) in EphA2 LBD, and b^3(127-131), b^4(212-216), b^5(521-526), b^6(547-550), b^7(558-559), b^8(627-629) in gH. The disulfide bonds are indicated with yellow numbers, and N-linked glycosylation sites with hexagons (green with black border – built in our structure; green with gray border – built in the PBD accession code 7CZF [1]; white, with black borders – remaining, predicted sites). Signal peptides at the start of each protein are represented as white boxes with grey lines, transmembrane anchor domains in EphA2 and gH as dark grey boxes, and double strep tag for affinity purification on gL and EphA2 LBD as half circles. **B)** The structure of the tertiary complex is represented as molecular surface and cartoon model (EphA2 LBD in purple, gL in blue and gH in grey). The N- and C- termini of each protein are labelled with letters "N" and "C", respectively. The four domains of gH are marked with roman numbers on the left side, and putative locations of the viral and cellular membranes with dashed arrows (black and purple, respectively). The hinge / linker region on gH is indicated with a grey arrow, and putative position of the unresolved J helix in the LBD with a pink * symbol.

Figure 2: The binding interface between EphA2 LBD and HHV-8 gH/gL

1097   Figure 2 legend

1098   **A)** The mixed β-sheet formed by strands of gH, gL and EphA2. The strands in gH and gL are labeled as
1099 $β_{number}$, while the EphA2 LBD strands are marked using the single-letter nomenclature assigned for the
1100   first solved structure of the EphB2 LBD 1KGY [2]. The same coloring scheme as in Figure 1 is applied
1101   (left panel). View are the gH/gL and EphA2 binding interface from the other side with the inlet
1102   illustrating the channel formed by the EphA2 and gL strands ('roof') that accommodates the gL N-
1103   terminal 'tail', reinforced by polar interactions between R103[EphA2] and E52[gH] ('base') (right panel).
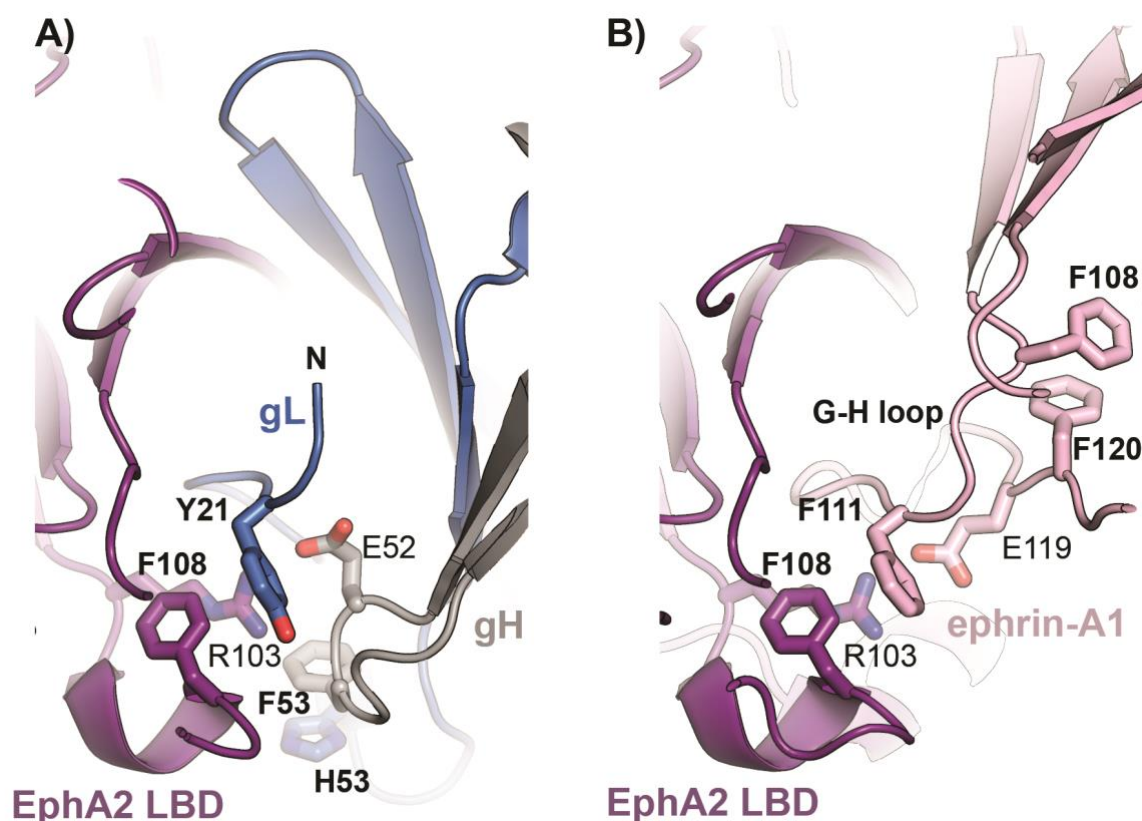1104   **B)** Locations of the point mutations introduced in EphA2 (R103A) and gH (E52A, E52R), and N-linked
1105   glycosylation sites in EphA2 (N57, A190N) and gL (Q30N, D68N) are indicated, and their side chains are
1106   shown as sticks. The same coloring scheme as in Figure 1B is applied.
1107   **C)** Sensorgrams recorded for WT EphA2 ectodomain of LBD binding to immobilized gH/gL by biolayer
1108   interferometry. A series of measurements using a range of concentrations for EphA2 ectodomain and
1109   LBD, respectively, was carried out to obtain the Kd for the WT proteins. Experimental curves (colored
1110   traces) were fit using a 1:1 binding model (black traces) to derive equilibrium K_d values.
1111   **D)** Sensorgrams recorded for EphA2 variants binding to immobilized gH/gL variants by biolayer
1112   interferometry. Single experimental curves obtained for EphA2 ectodomain concentration of 62.5 nM
1113   plotted to show the effect of the, respectively, EphA2 mutations, gL mutations, and gH mutations on
1114   binding.

Figure 3: Structural mimicry between HHV-8 gH/gL and ephrin ligands

ephrin-A1	T	L	K	G	E	F	K	E	G	123
ephrin-A2	S	L	G	F	E	F	R	P	G	146
ephrin-A3	S	L	G	Y	E	F	H	A	G	142
ephrin-A4	S	L	G	F	E	F	L	P	G	128
ephrin-A5	S	L	G	F	E	F	R	P	G	134
HHV-8 gH	S	I	E	L	E	F	N	G	T	56

Figure 3 legend

The EphA2 LBD from the EphA2 LBD – ephrin-A1 complex structure (PDB 3HEI) was superimposed onto the EphA2 LBD from our complex. The same coloring scheme for gH/gL and EphA2 is applied as in the previous figures, with the GH[ephrin-A1] loop shown in pink. For clarity, only the elements participating in the interactions are shown. The E119[ephrin-A1] is indicated. Sequence alignment of a GH loop segment of ephrin-A ligands, and the HHV-8 gH sequence is displayed to highlight the conservation of the glutamic acid that forms SBs with the EphA2[R103] (E52[gH] and E119[ephrin-A1]).

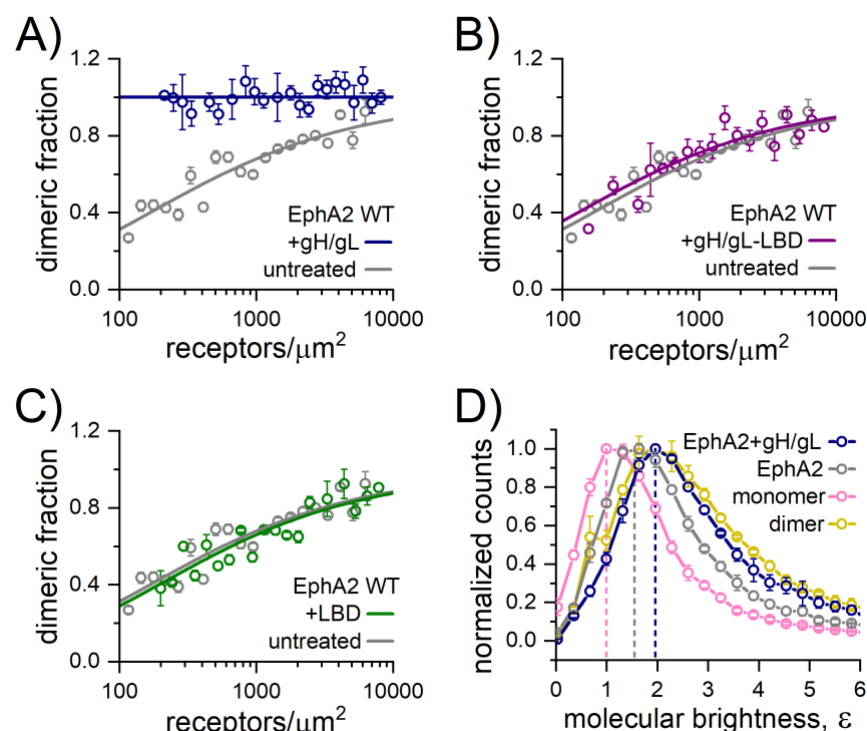1126 **Figure 4: HHV-8 gH/gL induces constitutive EphA2 dimerization.**

1127
1128
1129 Figure 4 legend

1130 The FSI-FRET data measured in HEK293T cells (Fig. S8) were fit to dimerization models to generate
1131 dimerization curves by plotting the calculated dimeric fraction as a function of the total EphA2
1132 concentration. The binned dimeric fractions are shown along with the best-fit curve. The data
1133 measured for EphA2 WT in the presence of **(A)** 200 nM gH/gL, **(B)** 200 nM LBD, and **(C)** 200 nM gH/gL-
1134 LBD are compared to EphA2 WT data in the absence of ligand, which was previously reported [3].
1135 Soluble gH/gL induces constitutive EphA2 dimerization, as evidenced by the dimeric fraction of 1 at all
1136 measured EphA2 concentrations. Little to no difference in the dimerization curves were observed
1137 when in the presence of LBD and precomplexed gH/gL-LBD compared to untreated EphA2 WT which
1138 suggests that EphA2 LBD blocks the effect of gH/gL on EphA2 dimerization. **(D)** Fluorescence Intensity
1139 Fluctuation (FIF) measurements in HEK293T cells reporting on EphA2 WT-eYFP oligomer size in the
1140 absence or presence of 200 nM gH/gL. Histograms of molecular brightness (ε), measured in small
1141 regions of the basolateral membrane over all measured receptor concentrations, are compared to the
1142 published FIF data for the monomer control (LAT) and dimer control (E-cadherin). The maximum of the
1143 histogram for EphA2 WT in the presence of gH/gL shifts to higher brightness than for EphA2 WT in the
1144 absence of ligand and is very similar to that of the E-cadherin dimer control, which suggests that EphA2
1145 is a constitutive dimer in the presence of gH/gL, consistent with the FSI-FRET data.

Figure 5: The gH/gL induced EphA2 dimers on cells engage the 'dimerization' interface.
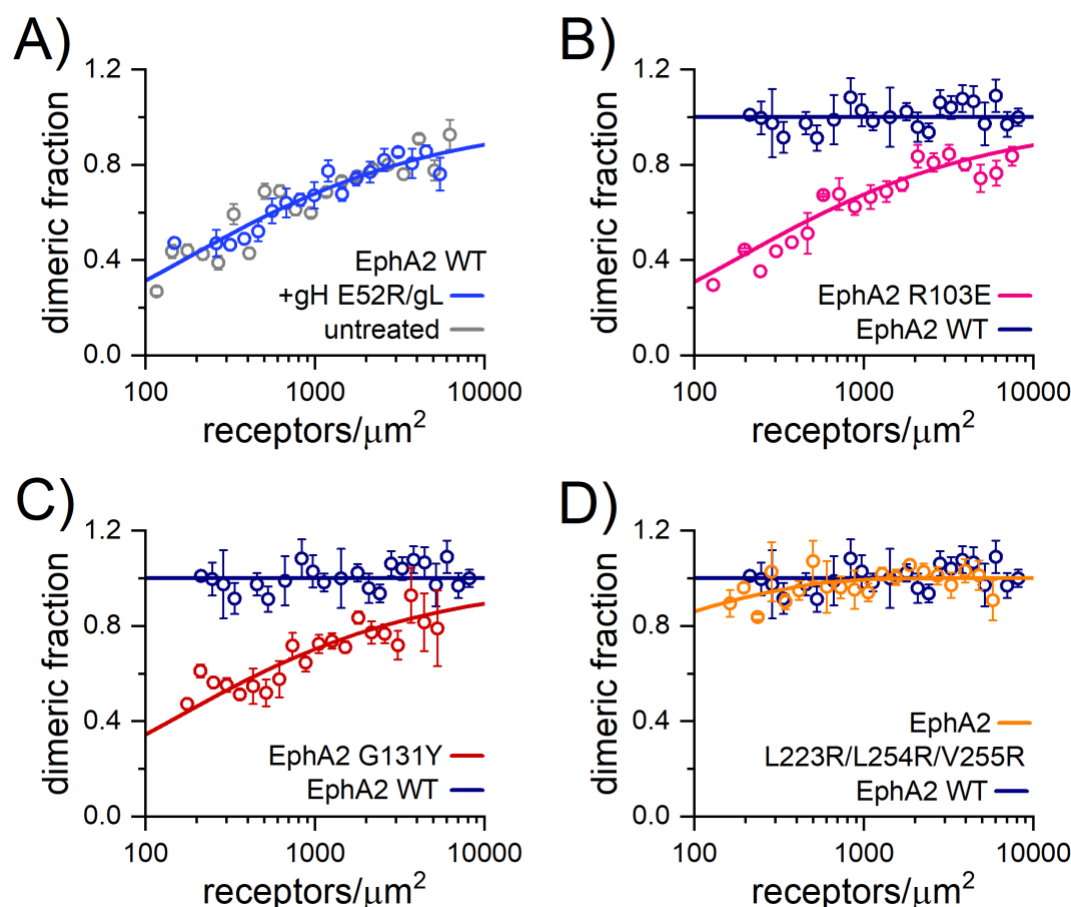

Figure 5 legend

Dimerization curves calculated from the FSI-FRET data for **(A)** EphA2 WT in the presence of 200 nM gH E52R/gL mutant with mutation in EphA2 binding, and for the EphA2 mutants **(B)** R103E[EphA2] mutant impaired in ligand binding, **(C)** G131Y[EphA2] mutant with mutation in DIN, and **(D)** L223R/L254R/V255R[EphA2] mutant with mutations in CIN. The data in A are compared to EphA2 WT data in the absence of ligand. The data in B-D were collected in the presence of 200 nM gH/gL and are compared to EphA2 WT in the presence of gH/gL (Fig. S8). No difference in the dimerization curve is observed with the mutated gH E52R/gL and thus does not induce constitutive EphA2 dimers as gH/gL does, which suggests impaired binding to EphA2. Large differences in the dimerization curves are observed for the R103E[EphA2] and G131Y[EphA2] mutants, but the effect of the triple L223R/L254R/V255R[EphA2] mutation is modest. This data indicates that gH/gL-bound EphA2 dimers interact mainly via the DIN (where G131 is engaged) but not via the CIN (where L223/L254/V255 are engaged) and that R103[EphA2] is important for gH/gL binding.

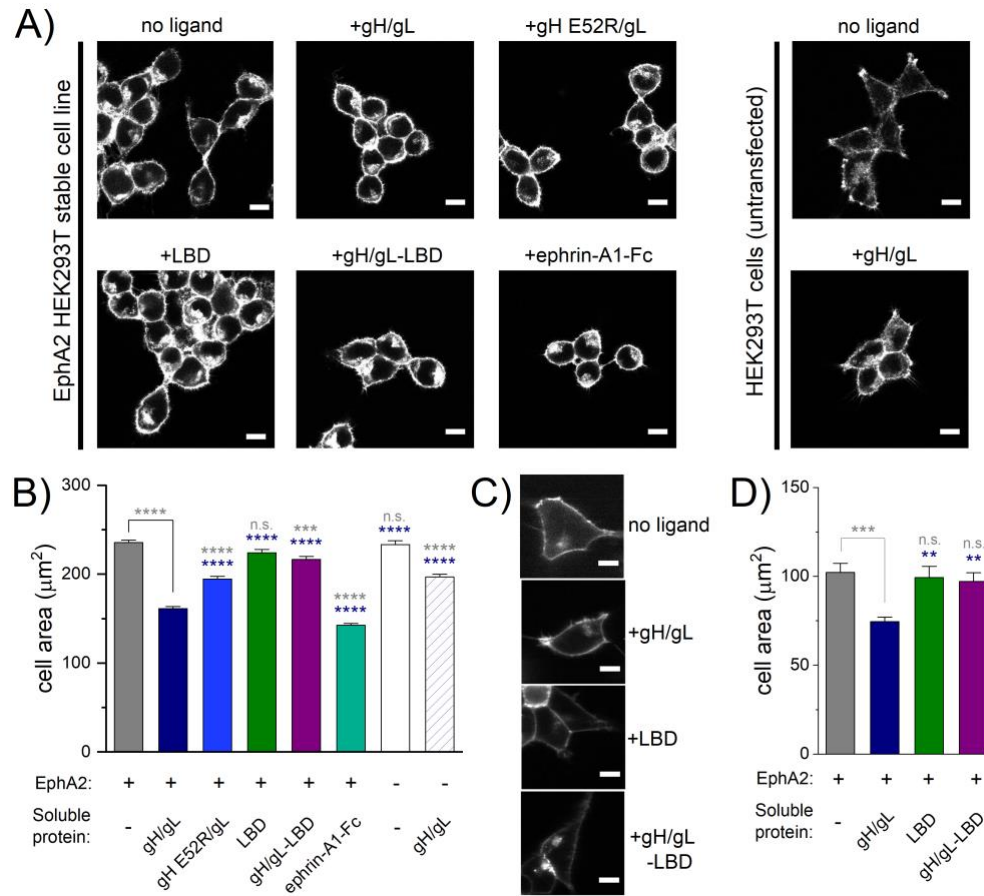## Figure 6: HHV-8 gH/gL stimulates EphA2-induced cell contraction.

Figure 6 legend

A) Images of fixed HEK293T cells stained for actin with rhodamine-conjugated phalloidin. The six images on the left were collected with HEK293T cells stably expressing EphA2 WT-eYFP and the two images on the right with HEK293T cells which do not express EphA2. Cells were stimulated with PBS (no ligand), 200 nM gH/gL, 200 nM gH E52R/gL, 200 nM LBD, 200 nM gH/gL-LBD complex, or 500 ng/mL ephrin-A1-Fc for 10 min prior to fixing with paraformaldehyde. Scale bar is 10 μm.

B) Histograms of the average cell areas and the standard errors determined from the images of fixed cells shown in panel A. In the presence of saturating gH/gL concentrations, the EphA2-eYFP-expressing cells are significantly smaller in size compared to the cases of no ligand, +gH E52R/gL, +LBD, and +gH/gL-LBD, but are larger than cells stimulated with ephrin-A1-Fc. Untransfected HEK293T cells experience a slight decrease in average cell area in the presence of gH/gL but not to the same extent as cells expressing EphA2. Statistical significance was determined by a one-way ANOVA and a Tukey's multiple comparison using the GraphPad Prism software ($P < 0.0001$ = ****, $P < 0.001$ = ***, $P < 0.01$ = **, $P < 0.1$ = *, $P \geq 0.1$ = n.s.). Statistics results in grey are compared to EphA2 no ligand and those in navy are compared to EphA2 + gH/gL.

C) Images of live HEK293T cells transiently transfected with EphA2 WT-eYFP in the absence or presence of 200 nM gH/gL, 200 nM LBD, or 200 nM gH/gL-LBD. Scale bar is 10 μm.

D) Histograms showing the average cell areas and the standard errors determined from the live cell images shown in panel C. In the presence of saturating gH/gL concentrations, the EphA2-eYFP-expressing cells are smaller in size compared to cells with no ligand, with LBD, and with gH/gL-LBD. Statistical significance was determined by a one-way ANOVA and a Tukey's multiple comparison using the GraphPad Prism software ($P < 0.0001$ = ****, $P < 0.001$ = ***, $P < 0.01$ = **, $P < 0.1$ = *, $P \geq 0.1$ = n.s.). Statistics results shown in gray when comparison is made compared to unliganded EphA2, and those in navy in comparison to EphA2 + gH/gL.

42

References

1. Su, C., et al., *Molecular basis of EphA2 recognition by gHgL from gammaherpesviruses.* Nat Commun, 2020. **11**(1): p. 5964.
2. Himanen, J.P., et al., *Crystal structure of an Eph receptor-ephrin complex.* Nature, 2001. **414**(6866): p. 933-8.
3. Gomez-Soler, M., et al., *Engineering nanomolar peptide ligands that differentially modulate EphA2 receptor signaling.* Journal of Biological Chemistry, 2019. **294**(22): p. 8791-8805.
4. Singh, D.R., et al., *The SAM domain inhibits EphA2 interactions in the plasma membrane.* Biochim Biophys Acta Mol Cell Res, 2017. **1864**(1): p. 31-38.
5. Singh, D.R., et al., *Intracellular Domain Contacts Contribute to Ecadherin Constitutive Dimerization in the Plasma Membrane.* J Mol Biol, 2017. **429**(14): p. 2231-2245.